NTNU – Trondheim
Norwegian University of
Science and Technology

Fluid Structure Interaction Simulation on an Idealized Aortic Arch

Thomas Bertheau Eeg

Master of Science in Product Design and Manufacturing
Submission date: June 2012
Supervisor: Leif Rune Hellevik, KT

Norwegian University of Science and Technology
Department of Structural Engineering

Assignment

"Fluid Structure Interaction Simulation on an Idealized Aortic Arch"

Aortic dissection is a condition where the first layer of the aortic wall is breeched causing bleeding between the layers or out of the aorta entirely. Aortic dissection has a high probability of death even if treated correctly. This study should look at blood flow in a idealized aortic arch as a precursor to later studies on the subject. The final goal is to establish a fluid-structure interaction model for physiological flow conditions in the aorta.

Suggested steps in achieving this are:

- Parameterization of an idealized geometry of the aortic arch
- Imposition of suitable boundary conditions
- Structural calculations of the vessel walls with dynamic and/or static loading
- Flow simulations with relevant boundary conditions
- FSI simulations of the idealized aortic arch ...

Preface

This study report describes the project conducted as my final Master's thesis concluding a 5-year integrated M. Sc. program in Mechanical Engineering at NTNU. The project was carried out for the Biomechanics group at the Department of Structural Engineering. The goal of the project was to study physiological flow in an idealized model of the human aortic arch including the three carotid arteries. Due to several technical difficulties along the way this model was further simplified.

I would like to thank my supervisor, professor Leif Rune Hellevik, for his guidance and help during this project. I am also deeply grateful to doctorate student Paul Roger Leinan for allowing me to use his previous work, as well as his technical and theoretical assistance throughout the duration of this study. In addition I would like to thank doctorate student Kamil Rehak for his technical help with meshing.

Thanks to Elisabeth Meland and Vinzenz Eck for making late nights at the office enjoyable.

Thomas Bertheau Eeg
June 11th, 2012
Trondheim, Norway

Sammendrag

Aortabuen er svært utsatt for hjerte- og karsykdommer, slik som disseksjon av aorta. Mange av risikofaktorene er grunnet fluid-strukturinteraksjonen mellom blodstrømmen og aortaveggen. Fluid-strukturinteraksjon (FSI) simuleringer er et nyttig verktøy i undersøkelsen av disse risikofaktorene. Målet med denne studien er å undersøke en forenklet modell for det fysiologiske strømningsbildet og legge til grunn for videre studier på hjertesykdommer i aortabuen. En 3-dimensjonal, idealisert FSI modell av aortaen ble laget ut i fra målinger funnet i literaturen. Denne modellen ble simulert ved hjelp av de kommersielle kodene Abaqus og Ansys Fluent, som ble koblet sammen av den akademiske koden Tango. Forsøk på å simulere geometrien som inkluderte truncus brachiocephalicus, den venstre arteria carotis communis og venstre arteria subclavia lyktes ikke. Derfor ble en noe mer forenklet modell simulert. Hovedfokuset ble lagt på undersøkelsen av grensebetingelser. Massestrømsbetingelse, resistansemodell eller varierende elastansemodell ble satt på innløpet, mens utløpet ble satt til null trykk, refleksjonsfri eller Windkessel. Massestrømsinnløp med Winkessel på utløpet ga de mest troverdige resultatene ettersom de andre innløpsbetingelsene ble uferdige approksimasjoner. Det kan ikke konkluderes noe om Ansys Workbench sin evne til å meshe for Tango grunnet manglende informasjon.

Abstract

The aortic arch is at risk of several cardiovascular diseases, such as aortic dissection. Many of these risk factors are due to the fluid-structure interaction that occurs in the aorta. Fluid-structure interation (FSI) simulations are a very useful tool in identifying these risks. The goal of this study is to obtain a simplified picture of healthy physiological flow and lay the foundation for further studies on cardiovascular diseases in the aortic arch. A 3-dimensional idealized FSI model of the aorta was constructed from measurements found in the literature. This model was simulated using the commerical codes Abaqus and Ansys Fluent, coupled with the in-house code Tango. Attempts at simulating the model geometry including the braciocephalic, left common and left subclavian carotid arteries were unsuccesful, so a simlified model of only the aortic arch was simulated. Emphasis was placed on the investigation of different boundary conditions. An imposed massflow condition, a pressure condition with resistance or a varying elastance model was set on the inlet and combined with zero pressure, reflection free or Windkessel outlet boundaries. The mass flow inlet with Windkessel outlet gave the most reliable results since the other inlets were mostly incomplete approximations. No conclusion could be drawn on the viability of Ansys Workbench as a meshing utility for studies using Tango, due to lack of information.

Contents

I Abbreviations

CV	Control Volume
DN	Dirichlet Neumann
FVM	Finite Difference Method
FEM	Finite Element Method
FSI	Fluid-Structure Interaction
FFT	Fast Fourier Transform
Hex	Hexahedral
IQN	Interface Quasi-Newton
NTNU	Norwegian University of Science and Technology
PWV	Pulse Wave Velocity
Tet	Tetrahedral
UDF	User-Defined Function
WK	Windkessel

II Nomenclature

Area	A	Pressure	P
Body forces	F_b	Pulse Wave Velocity	c
Characteristic impedance	Z_c	Resistance	R
Compliance	C	Strain	ε
Deformation	$\mathbf{u}$	Stress	σ
Density	ρ	Time	t
Displacement	$\mathbf{x}$	Traction stress	$\mathbf{t}$
Dynamic viscosity	μ	Velocity	$\mathbf{v}$
Elastance	$\mathcal{E}$	Volume	V
Mass flow	Q	Young's Modulus	E
Poisson's ratio	ν		

1 Introduction

The aorta is the main blood vessel in the human body. The placement of the aortic arch can be seen in figure 1a. It transports blood from the left ventricle of the heart to the rest of the body. The flow mechanics in blood vessels are known to cause several different diseases, such as aortic dissection.

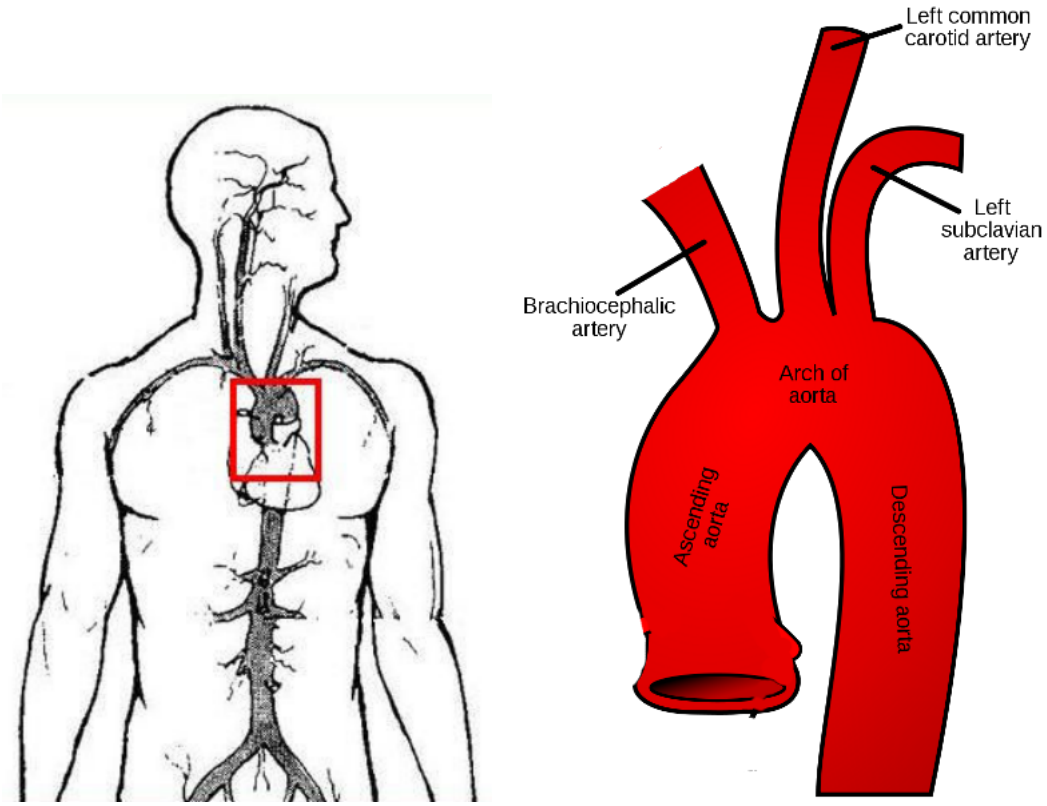

(a) Position of the aortic arch in the arterial network. Gao et al. [6]

(b) Representation of the aortic arch.

Figure 1: Position and geometry of the aortic arch. [1]

The aortic wall is made up of three layers: intima, media and adventitia. Unusual flow conditions like high blood pressure or atherosclerosis, as well as genetic disorders or trauma causing weaknesses in the aortic wall, can cause expansion of the aorta. This expanded region is called an aortic aneurysm. The layers can also tear causing blood to flow between them, called aortic dissection. The blood filled gap between the two layers will expand, forming a new channel referred to as the false lumen [7]. When this false lumen expands it could potentially block blood flow in the true aortic channel and/or eventually rupture.

According to the Stanford classification system a Type A dissection is classified as a dissection of the ascending aorta and Type B as occuring in the descending aorta. In

[1] Image source of fig. 1b : http://en.wikipedia.org

cases of Type B aortic dissection the survival rates after treatment range from 56% to 92% for 1 year and 48% to 82% for 5 years in different studies [17]. Hence, aortic dissection is studied at a large scale with several different focus points, to improve detection and treatment. This study will not consider pathological flow, but rather lay the methodical groundwork for further studies on the topic by simulating an idealized aortic arch during healthy conditions.

Vascular fluid mechanics represent several challenges in the form of complex geometries, pulsatile flow due to pumping of the heart and compliant vessel walls. Simulating only the flow field with rigid walls would miss significant flow features, such as the pressure wave propagation. FSI simulations may provide more accurate solutions, as compared to CFD [4] and 1-dimensional modelling, but still has limiting factors. It is very computationally expensive, which is severely limiting widespread use. The computational costs make simulating the entire arterial network within a reasonable time unfeasible. This means that whatever is outside our solution domain needs to be modeled with boundary conditions, which can be difficult to do. Numerical stability of the coupling is another challenge, as is evident in this study. In addition there are approximations that still have to be used. Blood is a non-Newtonian fluid with both fluid and solid components. It is usually approximated as continuous and Newtonian as this is much easier to model. Material properties also have to be approximated as these can be very patient specific and not readily availible.

There have been several FSI studies on the aortic arch focusing on different aspects of the problem on both idealized and patient-specific geometries [4, 6, 8, 11]. The current study considers a highly idealized geometry put together from measurements found in the literature, see sec. 4.2. The purpose of this study is to become acquainted with the solvers used and how they interact with the model. Previously the coupling procedure has been used to simulate geometries meshed with Gambit [9], but it is uncertain how long this will be a valid option and may need to be replaced. This study uses Ansys Workbench to build the geometry and mesh it to see if this is a viable alternative. Special emphasis is also placed on the development of suitable boundary conditions . This knowledge can then be applied to more complex situations later, see sec. 7. This is a qualitative and not a quantitative study, so the accuracy of the solutions is not considered as much as the trend of the solution.

This report is organized as follows. In section 2.1 the governing equations of the solvers are briefly described and the coupling procedure is summarized. The boundary condition models are derived in sec. 2.2. A walkthrough of the steps taken to solve the problem is given in section 3. Section 4 gives descriptions of the different cases considered and the motivation behind them. The results for the different cases are provided in sec. 5. Section 7 gives recommendations for improvements and adjustments that should be made to the methodology in future studies.

2 Theory

2.1 Model description

Fluid Model

The fluid part of the FSI is described by the Navier-Stokes equations. To simplify our calculations we assume incompressible flow ($\rho = \text{constant}$) and that blood is a Newtonian ($\mu = \text{constant}$) and continuous fluid. In Eulerian form and index notation this is given as in (1).

$$\rho_f \left(\frac{\partial v_i}{\partial t} + \frac{\partial v_i v_j}{\partial x_j} \right) = -\frac{\partial P}{\partial x_i} + \mu \frac{\partial}{\partial x_j} \frac{\partial v_i}{\partial x_j} + F_{bj} \tag{1a}$$

$$\frac{\partial v_i}{\partial x_i} = 0 \tag{1b}$$

Here v is the fluid velocity, ρ_f is the fluid density, μ is the fluid's dynamic viscosity, P the pressure and F_b are the body forces acting on the fluid. Gravity is not included in any of the calculations. In index notation i and j are integers from 1 to 3 representing the 3 dimensions.

Since we will employ the use of moving boundaries in the simulation we modify the momentum equation to account for this. According to the Fluent Manual [1] this means introducing the effects of the mesh velocity, v_g, into (1a).

$$\rho_f \frac{\partial v_i}{\partial t} + \rho_f \left(v_j - v_{g,j} \right) \frac{\partial v_i}{\partial x_j} = -\frac{\partial P}{\partial x_i} + \mu \frac{\partial}{\partial x_j} \frac{\partial v_i}{\partial x_j} + F_{bj} \tag{2}$$

These equations were solved by the black box implicit FVM solver Ansys Fluent. For details see, the Fluent Manual [1]. The walls are set as no-slip and Fluent handles the deformation and motion of the dynamic mesh.

The flow has Reynolds numbers high enough to be in the turbulent flow regime, with values $\sim$6000. It was however still modeled as laminar in the study, so no turbulence models were applied. This was done for simplicity since fully accurate quantitave results were not the goal of the study and turbulence models would only add to computational time required, without adding to the understanding of how the solution behaves. This could be included in later studies if deemed necessary.

Solid Model

The dynamic equilibrium equations for a solid are given below in index notation.

$$\frac{\partial \sigma_{ij}}{\partial x_j} + F_{bj} = \rho_s \frac{\partial^2 u_i}{\partial t^2} \tag{3}$$

Here σ_{ij} are the stresses, F_{bj} the body forces, ρ_s the wall density and u_i the deformation.

To complete the system we need a constitutive relation between the stress and strain. For a linear, isotropic material this is usually Hooke's law, which in Liu and Quek [10] is given as

$$\sigma = \mathbf{c}\varepsilon \tag{4a}$$

$$\begin{bmatrix} \sigma_{11} \\ \sigma_{22} \\ \sigma_{33} \\ \sigma_{23} \\ \sigma_{13} \\ \sigma_{12} \end{bmatrix} = \begin{bmatrix} c_{11} & c_{12} & c_{12} & 0 & 0 & 0 \\ & c_{11} & c_{11} & 0 & 0 & 0 \\ & & c_{11} & 0 & 0 & 0 \\ & & & \frac{(c_{11}-c_{12})}{2} & 0 & 0 \\ & sym. & & & \frac{(c_{11}-c_{12})}{2} & 0 \\ & & & & & \frac{(c_{11}-c_{12})}{2} \end{bmatrix} \begin{bmatrix} \varepsilon_{11} \\ \varepsilon_{22} \\ \varepsilon_{33} \\ \varepsilon_{23} \\ \varepsilon_{13} \\ \varepsilon_{12} \end{bmatrix} \tag{4b}$$

$$c_{11} = \frac{E(1-\nu)}{(1-2\nu)(1+\nu)} \ , \ c_{12} = \frac{E\nu}{(1-2\nu)(1+\nu)} \tag{4c}$$

$\mathbf{c}$ is here a symmetrical matrix. E is Young's modulus and ν is Poisson's ratio. These two material constants need to be found or approximated. ε is the strain vector and it can be written as a function of the deformation u_i, as is done in (5).

$$\begin{aligned} &\varepsilon_{11} = \frac{\partial u_1}{\partial x_1}, \ \varepsilon_{22} = \frac{\partial u_2}{\partial x_2}, \ \varepsilon_{33} = \frac{\partial u_3}{\partial x_3}, \\ &\varepsilon_{23} = \frac{\partial u_2}{\partial x_3} + \frac{\partial u_3}{\partial x_2}, \ \varepsilon_{13} = \frac{\partial u_1}{\partial x_3} + \frac{\partial u_3}{\partial x_1}, \ \varepsilon_{12} = \frac{\partial u_1}{\partial x_2} + \frac{\partial u_2}{\partial x_1} \end{aligned} \tag{5}$$

The solid model calculations are done with the black box FEM solver Abaqus.

Fluid Structure Interaction

The coupling between the structure and fluid components of the calculation is handled by the in-house code Tango. A detailed description of the coupling algorithms can be found in Degroote [5], but a summary of the relevant procedure is given in this section.

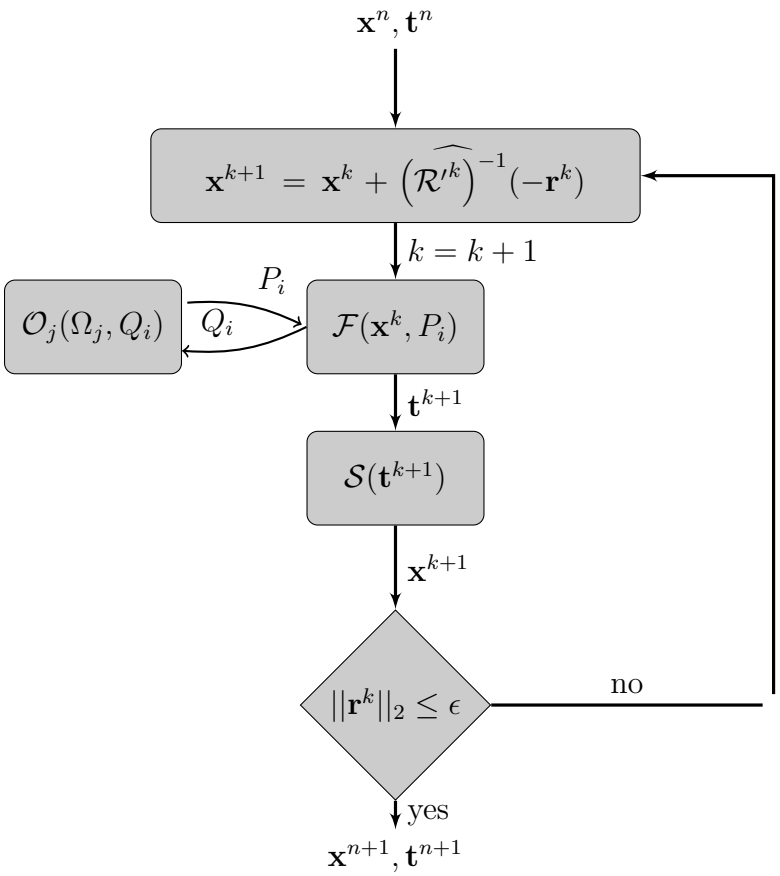

Figure 2: Schematic representation of fluid structure interaction coupling including the lumped boundary models. n is the timestep counter and k the subiteration counter. $\mathcal{F}$ and $\mathcal{S}$ represent the fluid and solid solvers respectively and $\mathcal{O}_j$ are the lumped boundary models. Leinan et al. [9].

The coupling is handled in a partitioned manner where the commercial code Ansys Fluent calculates the fluid domain and Abaqus the solid domain of the system. The problem is divided into separate parts using a Dirichlet Neumann (DN) decomposition. This means that the flow is solved with regard to a velocity of the fluid-structure interface and the solid is solved for a stress distribution on this interface. This way the interface is the only part of the problem that needs to be considered by both sides.

The general procedure for the solution is given in fig. 2. The notation used is

$$\mathbf{t} = \mathcal{F}(\mathbf{x}, P),\ \mathbf{x} = \mathcal{S}(\mathbf{t}) \tag{6}$$

This illustrates how the fluid solver, $\mathcal{F}$, takes in the displacement of the fluid structure interface, $\mathbf{x}$, and returns the traction stress distribution, $\mathbf{t}$. The solid solver, $\mathcal{S}$, then uses the traction stress distribution and calculates for the displacement of the interface. The lumped models, $\mathcal{O}_j$ (see section 2.2), are inserted into the fluid solver using the mass flow and returning a pressure to be imposed on the fluid boundary, Ω. Using this we can state that the FSI problem becomes (7).

$$\mathcal{R}(\mathbf{x}) = \mathcal{S} \circ \mathcal{F}(\mathbf{x}, P) - \mathbf{x} = 0 \tag{7}$$

$\mathcal{R}$ is the residual operator in the root finding problem. Since Tango utilizes two black box solvers it is difficult to get their exact Jacobian matrices. These thus have to be approximated. The system is solved by quasi-Newton iterations so that the displacement of the interface is calculated by

$$\mathbf{x}^{k+1} = \mathbf{x}^k + \widehat{\left(\mathcal{R}'^k\right)}^{-1}(-\mathbf{r}^k) \tag{8}$$

Here $\widehat{\left(\mathcal{R}'^k\right)}^{-1}$ is the approximation of the inverse Jacobian of the residual operator. k is the subiteration counter and $\mathbf{r}^k$ is the residual. When the L2-norm of the residual is lower than the convergence criteria, $||\mathbf{r}^k||_2 \leq \epsilon$, the new timestep is updated. Verification, validity and stability analysis of these methods can be found in Degroote [5].

2.2 Boundary Conditions

Reflection Free Boundary

The reflection coefficient of a boundary is given in (9).

$$\Gamma = \frac{R - Z_c}{R + Z_c} \tag{9}$$

R is a resistance on the boundary and Z_c is the characteristic impedance of the system, defined as (10).

$$Z_c = \frac{\rho c(P)}{A} \tag{10}$$

To obtain a reflection free boundary condition we set the reflection coefficient to zero, $\Gamma = 0$. This is true when $R = Z_c$. Using this we can derive a discrete equation for the outlet condition, (11).

$$P^{n+1} = P^n + Z_c\left(Q^{n+1} - Q^n\right) \tag{11}$$

Windkessel Model

The purpose of a Windkessel model is to approximate the behavior of the peripheral system. The peripheral system means anything outside our computational domain, and the effects are modeled and imposed on the boundary to simulate physiological behavior. Below is a derivation of the 2 element Windkessel model.

The idea is that the mass flow into a blood vessel can be approximated by the volume expansion of that vessel due to interior flow, and the mass flow to that vessel's peripheral system. This is mathematically given in (12) as a volume flux, since the density can be removed everywhere.

$$Q = \frac{dV}{dt} + Q_p = C\frac{dP}{dt} + \frac{P - P_0}{R} \tag{12}$$

Here C is the compliance, defined as $\frac{dV}{dP}$. The compliance is a measure of how much the vessel wall will deform with changes in pressure. Rearranging this we get the two element Windkessel model

$$\frac{dP}{dt} + \frac{P - P_0}{\tau} = \frac{Q}{C}, \tau = RC \tag{13}$$

A three element Windkessel model also includes an impedance, Z_c. Doing so helps absorb the high frequency pulse waves. Including this we get the differential equation for a three element WK.

$$\frac{dP}{dt} + \frac{(P - P_0)}{\tau} = Z_c\frac{dQ}{dt} + Q\frac{dZ_c}{dt} + Q\left(\frac{1}{C} + \frac{Z_c}{\tau}\right) \tag{14}$$

This differential equation must be solved at the boundaries where the lumped models are prescibed.

Using implicit backward Euler to discretize (14) we end up with an equation for P at our current timestep. No superscript denotes previous timestep, while $n+1$ is the current timestep.

$$P^{n+1} = \frac{1}{\left(1 + \frac{\Delta t}{\tau}\right)}\left[P + \frac{P_0}{\tau}\Delta t + Z_c\left(Q^{n+1} - Q\right) + Q^{n+1}\Delta t\left(\frac{1}{C} + \frac{Z_c}{\tau}\right)\right] \tag{15}$$

Here $\frac{dZ_c}{dt}$ is neglected due to the linear wall elasticity and small changes in Z_c. Z_c is calculated by (10).

Following Beulen et al. [3] we can calculate the coefficients for a physiological pressure drop.

$$Z_c + R = \frac{\bar{P}}{\bar{Q}} \tag{16a}$$

$$C = \frac{\tau}{R} \tag{16b}$$

$\bar{P}$ and $\bar{Q}$ denote the mean pressure and mean volume flow respectively, while τ is a time scale. For physiological pressure drops Beulen et al. suggests τ =1.5 s.

Resistance Model

The resistance model is an attempt at obtaining aortic flow conditions by modeling the ventricular pressure and including a source resistance, R_s, to prevent backflow. The idea is that the resistance should force reflection of the backward traveling waves going into the ventricle. This is modeled as

$$P = P_{LV} + R_s Q \tag{17}$$

P is the pressure prescribed at the inlet, P_{LV} is the ventriclur pressure and Q is the volume flux over the boundary. To control the reflection the resistance has to be set accordingly. The reflection coefficient is defined as in (11). The resistance can then be calculated as a function of the characteristic impedance Z_c. Ideally the resistance should be variable in time to simulate complete resistance to flow as the aortic valve is closed, and very small resistance when it is open. This would mean that $R_s \to \infty$ in order to let $\Gamma \to 1$.

Time - Varying Elastance Heart Model

The varying elastance model was first introduced by Suga and Sagawa [16] in 1972 and is well established. The model used here is an expanded version, including a source resistance. The model can be found in Mynard et al. [12], but is briefly discussed below.

$$P(t) = \mathcal{E}(t)\left[V(t) - V_0\right] + R_s Q \tag{18}$$

The model is used to prescribe an inlet pressure and is given by the relation in (18). P is the inlet pressure, $\mathcal{E}$ the time-varying elastance, V the volume of the heart, V_0 the unstressed volume, Q the volume flow rate and R_s is the source resistance. The source resistance can be expressed as $K_s\mathcal{E}(V - V_0)$ giving the final equation.

$$P(t) = \mathcal{E}(t)\left[V(t) - V_0\right]\left[1 + K_s Q\right] \tag{19}$$

For our cases $Q < 0$ as this is inflow into the domain, and the normal vector is pointed out of the domain.

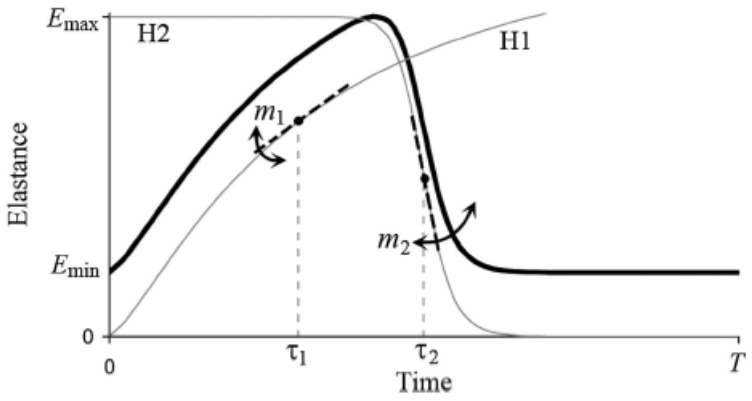

Figure 3: Two-Hill function used to describe the elastance time history in terms of its variables. From [12].

The time-varying elastance is described by the Two-Hill function. This is a function consisting of two combined "hills", one modelling the contraction and the other the

relaxation of the heart. It can be viewed in figure 3, which also depicts how the constants affect the model. The function is given by

$$\mathcal{E} = k\left(\frac{g_1}{1+g1}\right)\left(\frac{1}{1+g_2}\right) + \mathcal{E}_{\min} \tag{20a}$$

$$g_1 = \left(\frac{t}{\tau_1}\right)^{m_1},\ g_2 = \left(\frac{t}{\tau_2}\right)^{m_2} \tag{20b}$$

$$k = \frac{\mathcal{E}_{\max} - \mathcal{E}_{\min}}{\max\left[\left(\frac{g_1}{1+g1}\right)\left(\frac{1}{1+g_2}\right)\right]} \tag{20c}$$

The model uses several coeffecients. These are taken from Mynard et al. [12] and are given in table 1.

Table 1: Parameters used in the varying elastance heart model, taken from Mynard et al. [12]. T = 0,89 s

Parameter	**Symbol**	**Units**	**Left Ventricle**
Source resistance coefficient	K_s	10^{-9} s/mL	4
Minimal elastance	$\mathcal{E}_{\min}$	mmHg/mL	0,08
Maximal elastance	$\mathcal{E}_{\max}$	mmHg/mL	3,00
Residual volume	V_0	mL	10
Initial volume	V^0	mL	135
Contraction rate constant	m_1	-	1,32
Relaxation rate constant	m_2	-	27,4
Systolic time constant	τ_1	s	0,269T
Diastolic time constant	τ_2	s	0,452T

Combined with the fact that $Q = \frac{dV}{dt}$ we can discretize and solve these equations. Using the same discretization, but with $Q < 0$, we get

$$V^{n+1} = V^n + \frac{1}{2}\left(Q^{n+1} + Q^n\right)\Delta t \tag{21a}$$

$$P^{n+1} = \mathcal{E}^{n+1}\left(V^{n+1} - V_0\right)\left[1 + K_s Q^{n+1}\right] \tag{21b}$$

Using Q from the inlet of the domain is however a flaw. The volume flow into the left ventricle should be used, which is a combination of flow over the mitral valve and the backflow across the aortic valve. A rough approximation is possibly to use the volume flux over the boundary and return the heart volume to its initial state after each cycle. The validity of this is examined in section 5.3.

Valve Model

Mynard et al. [12] propose a valve model to approximate the valve motion due to pressure differences in the left ventricle and the aorta. A more complete model is given in their

paper, which accounts for damaged valves etc., but since this study deals with healthy conditions this was not considered.

The pressure difference is approximated by the Bernoulli equation. This relation includes the Bernoulli resistance (B) which models losses due to convection and the inertance (L) modelling blood acceleration, giving (22).

$$\Delta P = BQ|Q| + L\frac{dQ}{dt} \tag{22a}$$

$$B = \frac{\rho}{2(A_{\text{ann}}\zeta)^2}\ ,\ L = \frac{\rho l_{eff}}{A_{\text{ann}}\zeta} \tag{22b}$$

A_{ann} is the area of the annulus the heart model is placed at and l_{eff} is an effective length. The effective length was not given, but is assumed to be the length over the heart valve. They were set to 314e-6 m^2 and 0.01 m respectively. The differential equation for the opening valve motion is

$$\frac{d\zeta}{dt} = (1-\zeta)K_{vo}(\Delta P - \Delta P_{\text{open}}) \tag{23}$$

where ζ is the valve state, $\zeta = 1$ being open and $\zeta = 0$ closed. K_{vo} is the opening rate coefficient and ΔP_{open} the pressure difference required to open the valve. For closing the equation becomes

$$\frac{d\zeta}{dt} = \zeta K_{vc}(\Delta P - \Delta P_{\text{close}}) \tag{24}$$

A test case was constructed to see if it gave similar results. The pressure difference ΔP was set as a sinusoidal wave with increasing amplitude, i.e. $\Delta P = 2t\sin(\pi 1.6t)$ mmHg. The valve model then calculated its state from this. The results can be viewed in figure 4. The results correspond to those found by Mynard et al. [12].

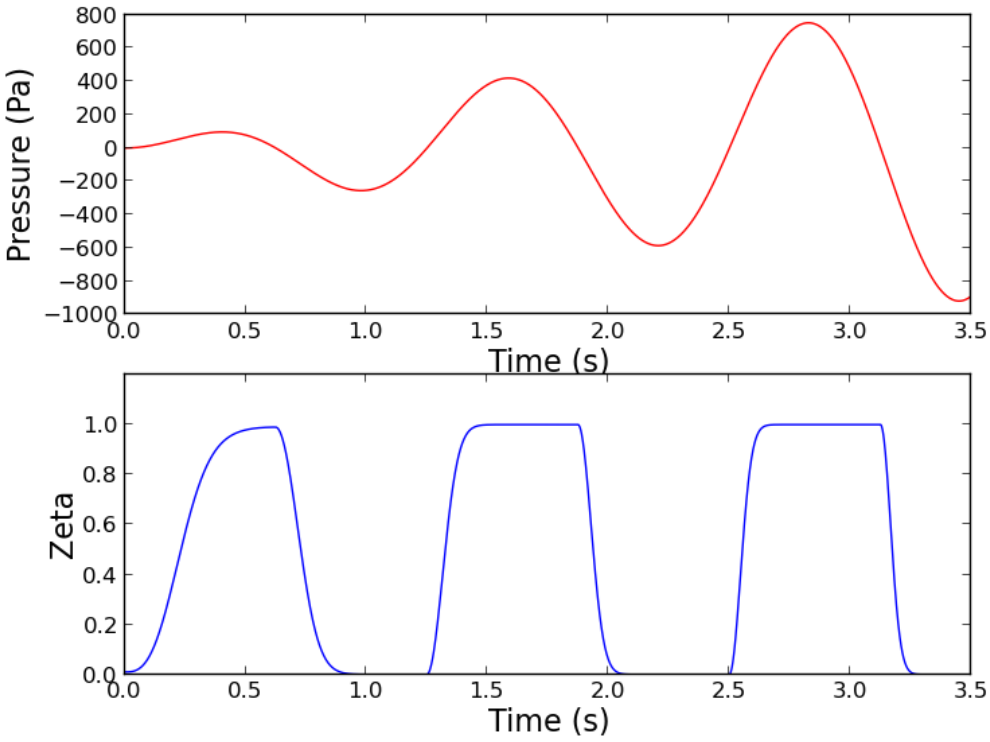

Figure 4: Valve state according to the differential equations. Above figure [red] is time history of a set ΔP i Pa. Below [blue] is the time history of the valve state ζ.

3 Method

The initial problem went through the following steps:

- Parameterize and create geometry
- Mesh geometry
- Solid model solved with Abaqus as standalone system
- Fluid model solved with Fluent as standalone system
- Solid model solved with Abaqus as CSM problem through Tango
- Fluid model solved with Fluent as CFD problem though Tango
- Solved FSI problem with Tango

When the FSI of the full idealized arch failed to run (sec. 5.2), a test case was constructed with a tube geometry and run through the same steps, see sec. 4.1. When this calculation was successful, the same parameters and conditions were applied to the full model. This did not resolve the issue. The full model's mesh was then rebuilt with better

quality and hexahedral, instead of tetrahedral, elements for the solid and tet elements for the fluid. The boundary conditions for these cases were $\sin^2$ velocity inlets and 0 pressure outlets. Since simulations were still unsuccessful, the full geometry was altered by removing the three carotid arteries from the model, see sec. 4.3. Boundary conditions were then investigated for our simplified geometry.

4 Case Description

4.1 Simple Tube

A simple test case was set up and run using Tango. A straight tube was modeled after the descending aorta to achieve a measure of relevance. Parameters for the simulation were found in the literature [9, 13] and are presented in table 2. Many different parameters have been used in the literature since accurate data can be difficult to obtain and possibly patient specific. These are therefore to be viewed as approximations. The simulations were run with $\Delta t = 0.005$ s.

Table 2: Model parameters for all simulations

Parameter	**Symbol**	**Value**
Dynamic viscosity	μ	$3 * 10^{-3}$ Pa s
Density of blood	ρ_f	1050 kg/m^3
Wall density	ρ_s	1200 kg/m^3
Poisson's ratio	ν	0.49
Young's modulus (Linear)	E	$5.3 * 10^5$ Pa

4.1.1 Geometry and Mesh

The tube was modeled after the descending aorta with a inner diameter $D_i = 20.5$ mm, wall thickness $\Delta r = 1$ mm and length $L = 140$ mm.

A mesh consisting of tetrahedral cells was created for the fluid model, fig. 5c. For the solid model two seperate meshes were created, one using brick elements (fig. 5a) and another with tetrahedral elements (fig. 5b). The latter was used to see if Tango could use continuous tet elements, as this was not listed in the Tango Manual [2].

(a) Brick C3D8 Elements

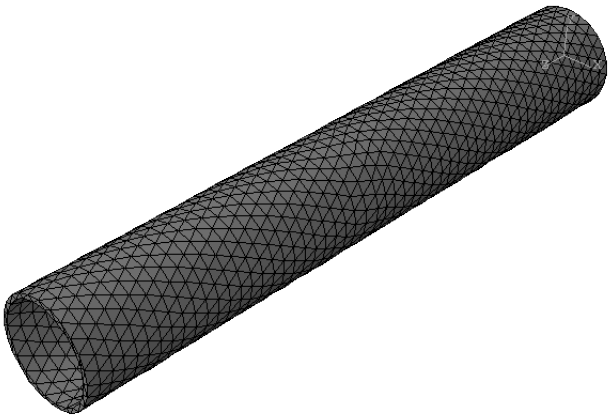

(b) Tet C3D4 Elements

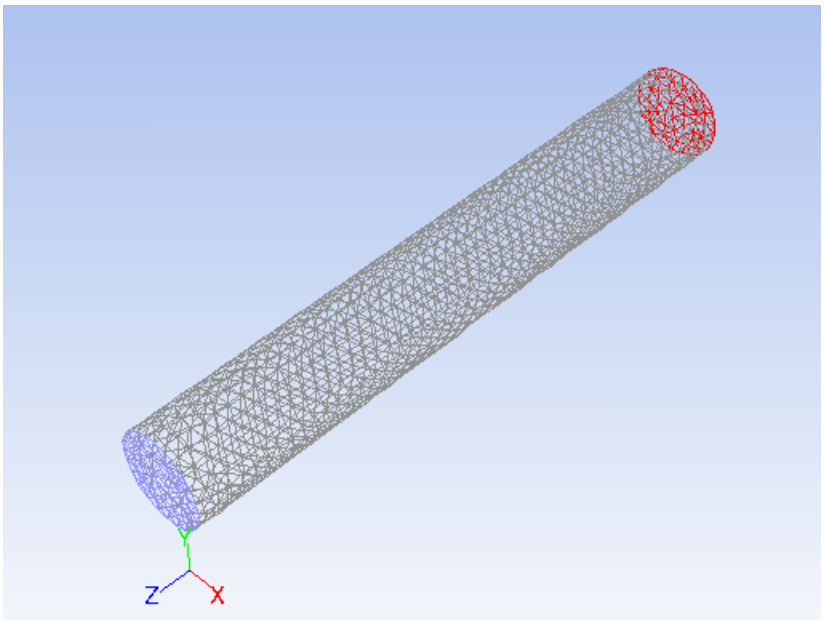

(c) Fluid mesh consisting of tet F3D4 elements

Figure 5: Meshes used in the test cases of a straight tube.

4.1.2 Boundary Conditions

For this case a square sine wave was prescribed as a velocity normal to the inlet. As this was a test case there was no need for physiological conditions.

$$v_{inlet}(t) = 0.1\sin^2(5\pi t) \tag{25}$$

The outlet was set to a pressure outlet with 0 pressure. Both the inlet and the outlet was able to expand freely in the radial direction, but constrained lengthwise and rotationally.

4.2 Aortic Arch

4.2.1 Geometry and Mesh

The geometry analyzed is an idealized aortic arch, including ascending and descending aorta and the bifurcations to the brachiocephalic, left common and left subclavian carotid arteries. The inner geometry of the aorta was taken from Redheuil et al. [14] for an average male in his twenties. The measurements for the carotid arteries were given in Stergiopolus et al. [15]. Wall thickness was taken from Pahlevan and Gharib [13] at specified points, see table 3. Since both the inner measurements and the wall thickness was given at discrete points, a smooth transition used between them. For simplicity the carotid arteries were placed in line, and perpendicular to the centerline, on the top of the aortic arch. They are also modeled as 40 mm from the outlet to the centerline of the arch to reduce the effect of the boundary conditions on the flow in the aorta. The model file is constructed in such a way that individual measurement changes to the geometry can be made, which causes the rest of the model to adjust accordingly. A 25 mm segment has been added to the inlet to allow the flow to develop and stabilize before entering the curvature.

The measurements of the model that were used can be viewed in figure 6 and table 3.

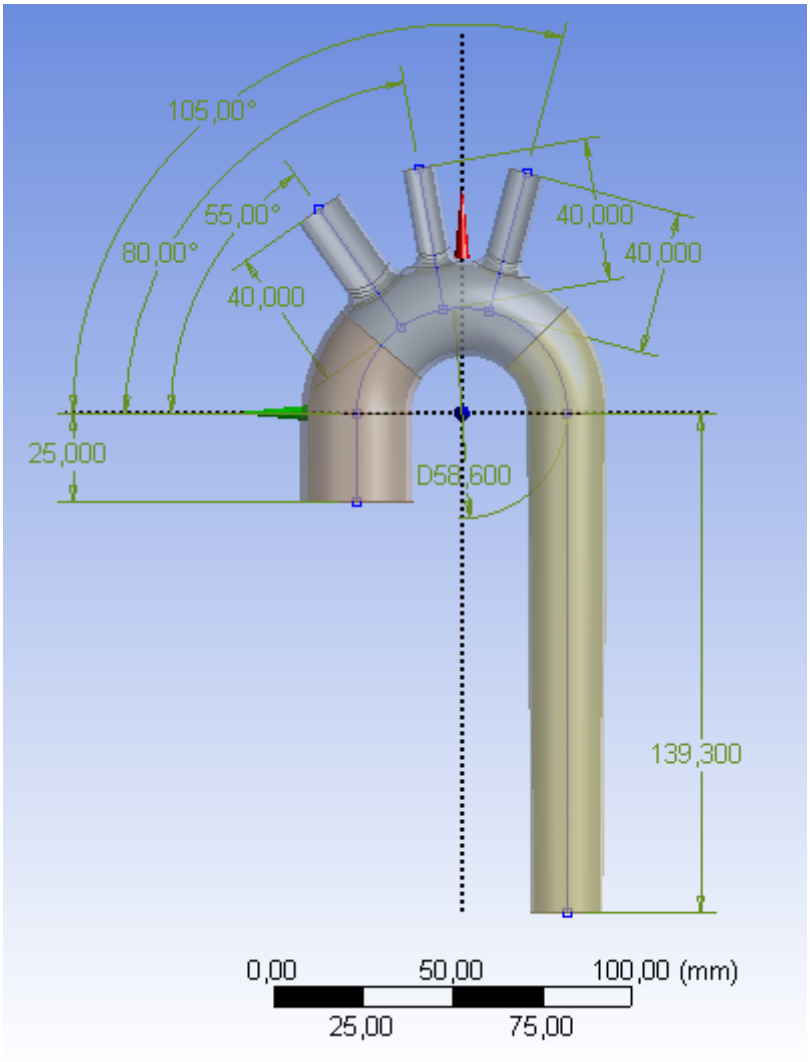

Figure 6: Geometry of the solution domain for the full model.

Table 3: Radial geometry measurements for cross sections of the model.

Artery	**Proxima Diameter**	**Prox. Wall Thickness**
Ascending Aorta	27.5 mm	1.4 mm
Aortic Arch	27.5 mm	1.4 mm
Descending Aorta	20.5 mm	1 mm
Abdominal Aorta	18.3 mm	0.9 mm
Braciocephalic Artery	12.4 mm	0.8 mm
Left Common Carotid Artery	7.4 mm	0.8 mm
Left Subclavian Carotid Artery	8.46 mm	0.8 mm

Meshes were attempted optimized in order to obtain a succesful simulation. The mesh of the highest quality was a hexahedral swept mesh for the solid and a tetrahedral mesh for the fluid. Combined these had a maximum skewness of 0.7.

4.2.2 Boundary Conditions

A $\sin^2$ wave, (25), was set as the velocity profile on the inlet and 0 Pa pressure on the outlets. Several other conditions were also set to see if this had any effect. These included reflection free and Windkessel models on the outlets, as well as no inflow, constant velocity and sinusoidal pressure waves at the inlet.

4.3 Simple Aortic Arch

Since the fluid-structure interaction simulations were unsuccesful for the aortic model including bifurcations (see sec. 5.2), a simpler geometry was made consisting of only the ascending aorta, aortic arch and descending aorta in the hope that this would be easier to simulate.

4.3.1 Geometry and Mesh

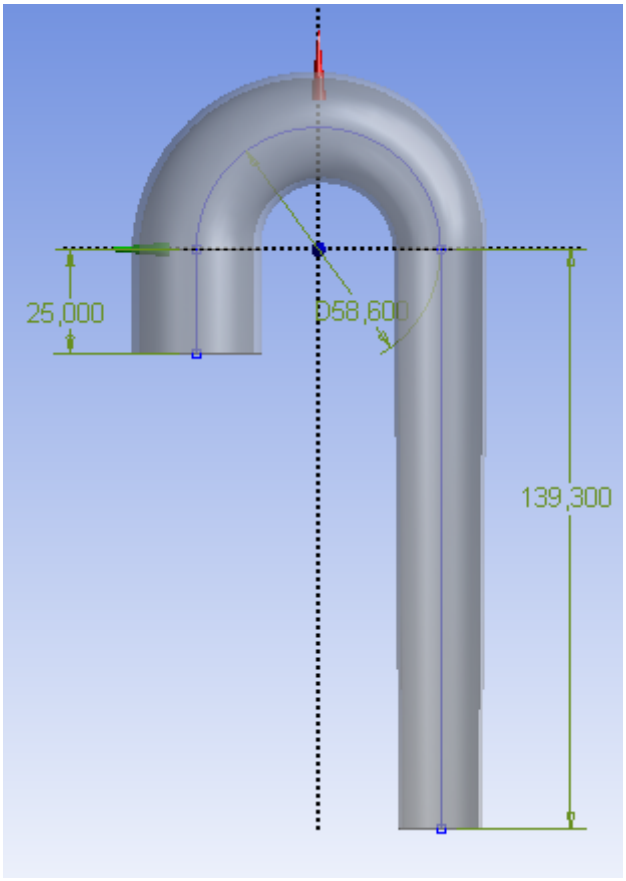

Figure 7: Model of the simplified aortic arch.

The carotid arteries were removed from the model found in section 4.2. Otherwise the parameters are the same for this case. The measurements can be seen in fig. 7 and table 3. The model parameters can be viewed in tab. 2.

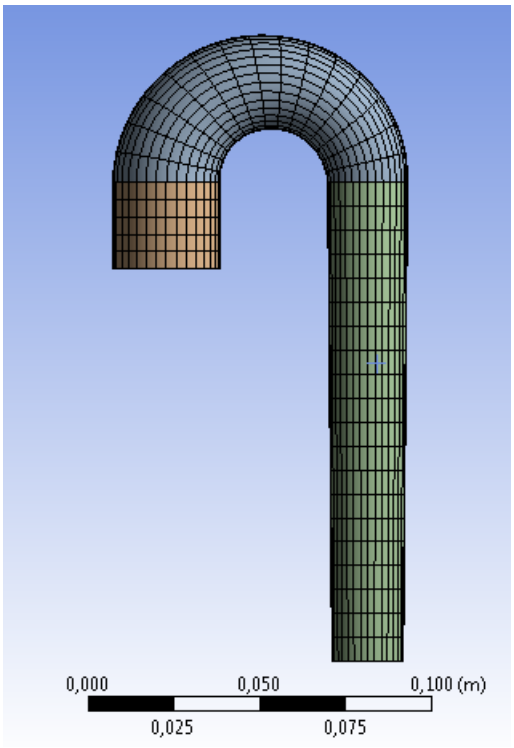

(a) Sideview

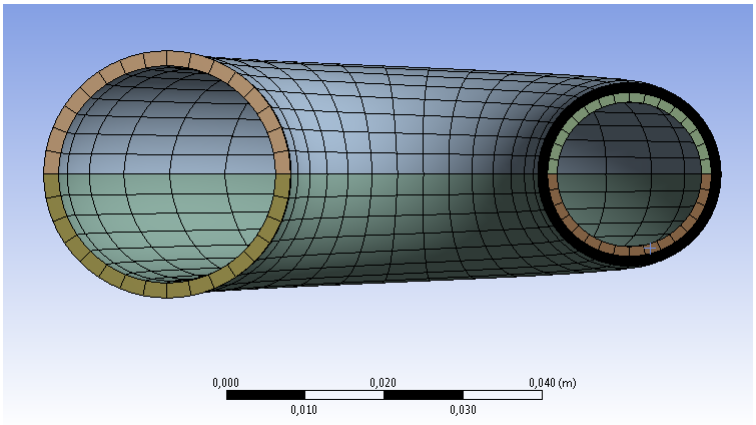

(b) View of inlet and outlet

Figure 8: Solid mesh: C3D8 linear brick element mesh created with Ansys Workbench.

For the solid part a hexahedral mesh was constructed using Ansys Workbench. Figure 8 shows two different views of the mesh. The mesh is constructed with C3D8 linear brick elements. The highest skewness of this mesh is 0.2.

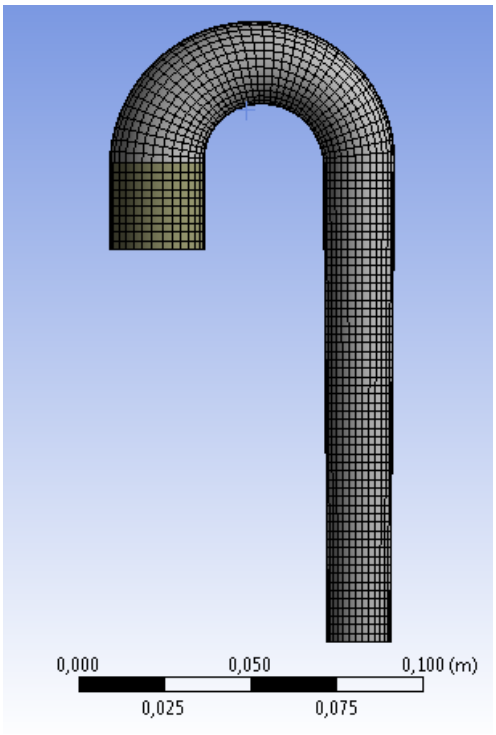

(a) Sideview

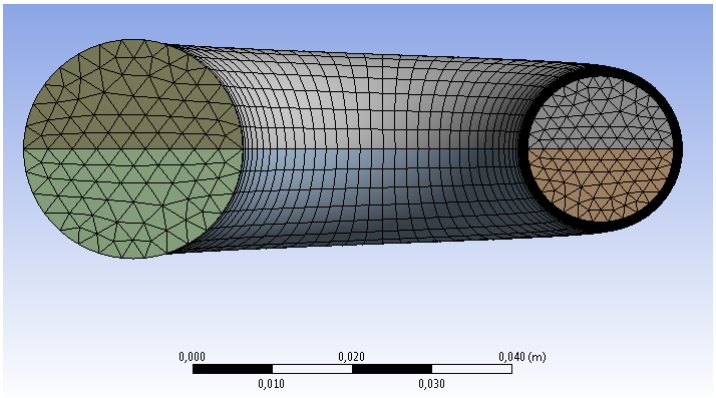

(b) View of inlet and outlet

Figure 9: Fluid mesh: F3D6 linear wedge element mesh created with Ansys Workbench.

The fluid mesh can be viewed in figure 9. It is comprised of F3D6 wedge elements with a maximum skewness of 0.4.

A coarser mesh was made with the same setup, but fewer divisons along the centerline for both the fluid and solid. This was used to obtain quicker results. This could be done as the exact results were not important to the study. Cases where the coarser mesh is used is specified.

4.3.2 Boundary Conditions

A linear elasticity model was used for the wall. See sec. 2.1 for the explanation of the constitutive relation.

A flow rate profile exiting the heart was found in Pahlevan and Gharib [13]. This was programmed as a UDF in Fluent and prescribed as a velocity inlet for case2, described

below.

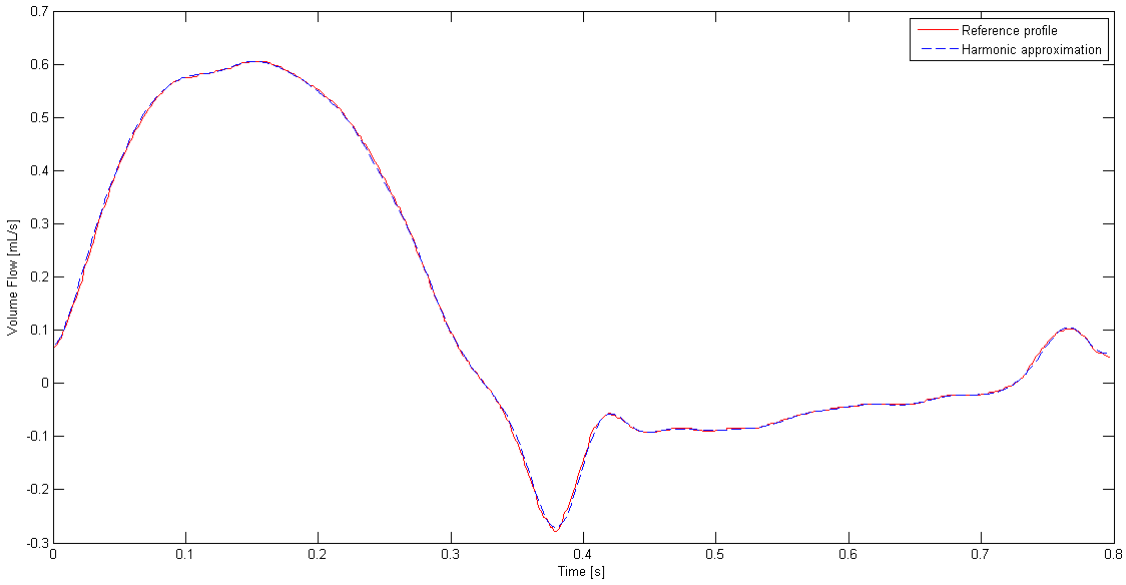

Figure 10: Velocity profile for the inlet. Profile [red] and 20 frequency harmonic approximation [blue]

In fig. 10 we can see the inlet profile as it is presented in Pahlevan and Gharib [13] and the harmonic approximation superimposed on top. The harmonic approximation utilizes 20 frequencies, found using FFT in Matlab. The original profile was extracted using Datathief.

Multiple cases of different combinations of boundary conditions were run to investigate the differences between them. The cases are presented below.

Case 1 At the inlet a $\sin^2$ wave with frequency 3.3 s^{-1} and amplitude of 0.6 m/s for the velocity is imposed. A reflection free outlet condition has also been set. $\Delta t = 0.005$ s.

Case 2 The physiological velocity inlet in figure 10 was used. At the outlet a reflection free boundary conditon was imposed.

Case 3 A 3 element Windkessel model, sec. 2.2, was used for the outlet. The model parameters were calculated with the method used by Beulen et al. [3]. The final parameters can be viewed in section 5.3.

For the inlet conditions a $\sin^2$ wave was utilized as a massflow inlet, with frequency 2.77 s^{-1} and an amplitude of 450 ml/s. After each pulse wave a pause of 0.5 seconds was inserted. This approximated the refill period of the heart cycle. This equals a mean flow of $\sim$ 95 ml/s over the heart cycle. The coarse mesh was used.

Case 4 The resistance model, see section 2.2, was applied on the inlet, and a 3 element Windkessel model at the outlet. A stationary R_s was set to $3Z_c$, which corresponds to

$\Gamma = 0.5$, since a time-variable R_s was unsuccesful. The ventricular pressure was set as a $\sin^2$ wave with frequency 2.77 s^{-1} and amplitude 150 mmHg. The coarser mesh was used in this case.

Case 5 The time-varying elastance heart model was set on the inlet according to sec. 2.2. The outlet was a Windkessel model. The coarser mesh was used.

5 Results and Discussion

The meshes have not been examined with mesh independence tests. As this is not a quantitive analysis results were not required to be mesh independent, but show trends in response to different boundary conditions. No inflation is applied near the boundaries either. This would severely affect the computational time needed and increase the chances of the mesh collapsing under the dynamic mesh condition. It was therefore decided that the boundary layers would not need to be resolved to that extent.

5.1 Tube

This was a test case to obtain a running simulation. This case could later be modified for the other geometries and conditions. The calculations were run with a timestep $\Delta t = 0.005$s. The results at the inlet and outlet of the tube can be viewed in figures 11 and 12 for the different meshes.

Hex Element Mesh

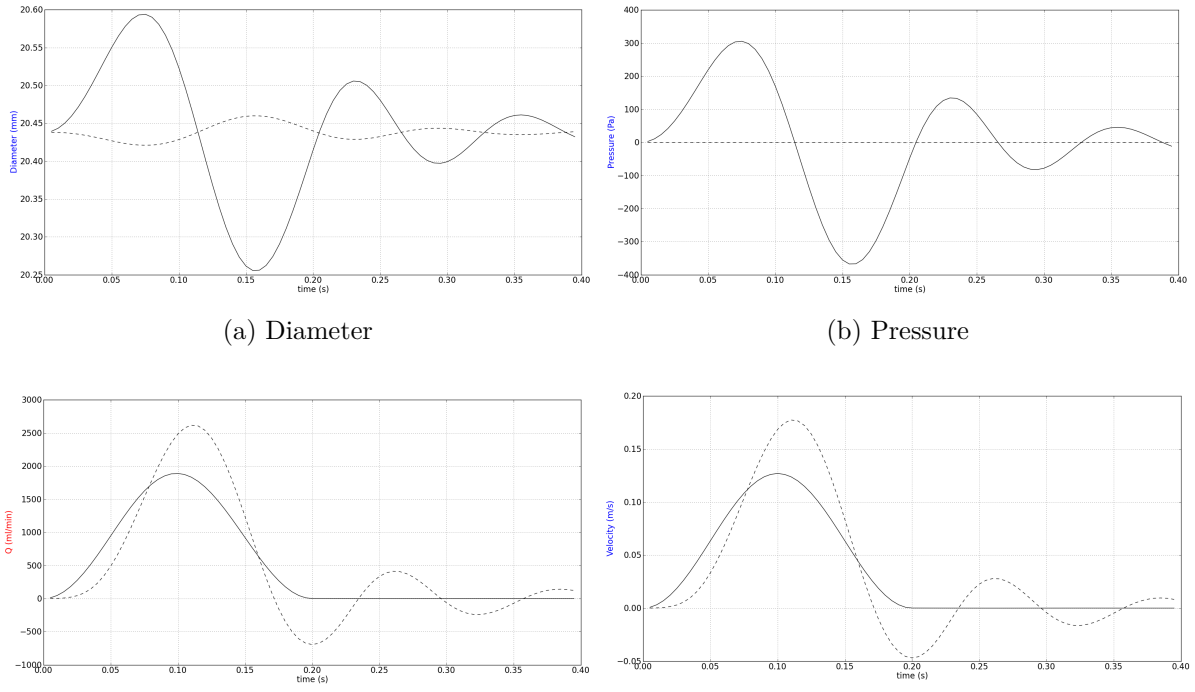

(a) Diameter

(b) Pressure

(c) Massflow

(d) Velocity

Figure 11: Results for the Hex mesh. 2D plots of 4 different parameters on the inlet [-] and outlet [- -] of the tube as a function of time.

The figures are graphical representations of 4 different parameters on each of the inlets and outlets as functions of time.

Since the pressure pulse is recorded at the outlet later than at the inlet we can deduce that there is propagation of the applied pressure pulse through the tube, and not an instantanious reacton. This is because of the compliant walls. We can see in fig. 11 that the inlet and outlet are not reflection free, but reflects the pulse back and forth between them. There is not total reflection of the wave so the pulse diminishes time. The nature of the reflections can be seen by the oscillating velocities at the outlet when there are no pulsewaves being forced on the inlet.

The hex case was run for a longer time than the tet mesh. This was done to examine the effects of the 0 mmHg pressure outlet, and once done would not need to be repeated for the other mesh.

Tet Element Mesh

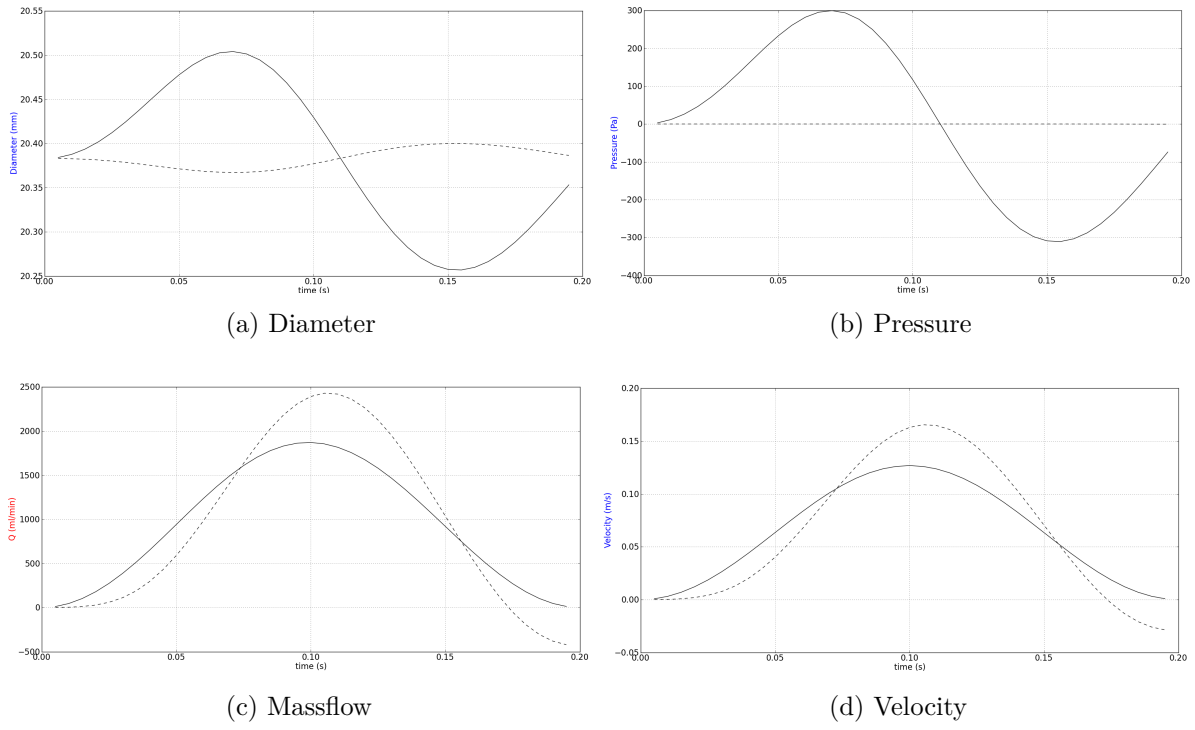

(a) Diameter

(b) Pressure

(c) Massflow

(d) Velocity

Figure 12: 2D plots of 4 different parameters on the inlet [-] and outlet [- -] of the tube as a function of time for the tet mesh.

The results are very similar for the tet element mesh, with differences that can be attributed to mesh refinement.

We can see the wave propagating through the pipe and then being reflected at the outlet as it does for the hexahedral mesh. It is evident that the simulation also works for continuous tet elements.

5.2 Aortic Arch

Computational Fluid Dynamics

For the $\sin^2$ velocity inlet the CFD results with rigid walls are given in fig. 13.

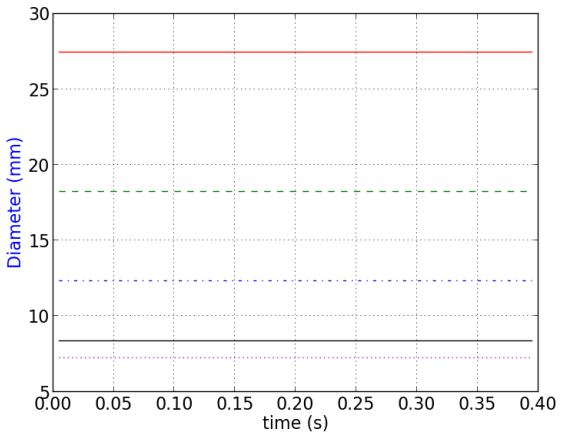

(a) Diameter in mm

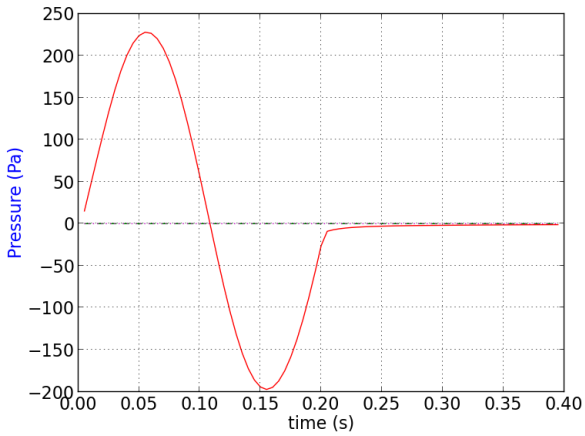

(b) Pressure in Pa

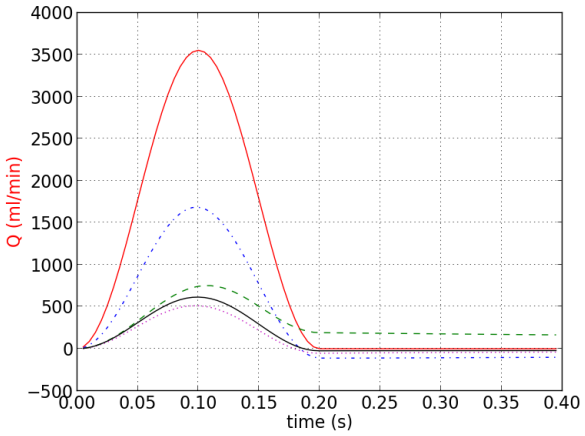

(c) Massflow in ml/min

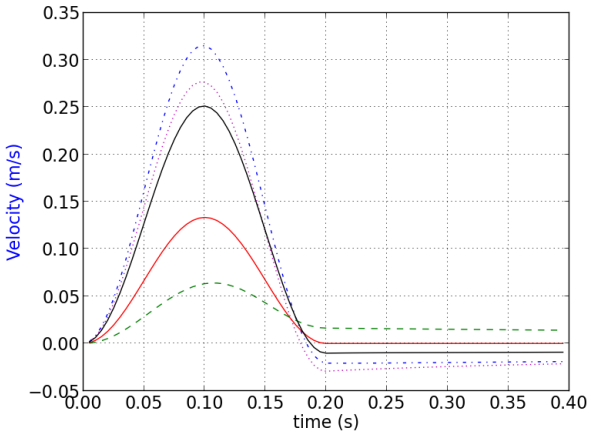

(d) Velocity in m/s

Figure 13: 2D plots of 4 different parameters as a function of time for each of the 5 boundaries: Inlet [red], outlet [green], brachiocephalic [blue], left common artery [purple] and left subclavian artery [black]. $\Delta t = 0,005$s.

With rigid pipe walls there is instantanious propagation of information through the geometry, meaning that the outlets immediately react to the inflow. This can be seen in figure 13d in that the velocities on the outlets increase as a reaction to the inlet flux without any delay. There is no pressure wave transporting the information downstream and hence also no reflection. We can see that the pressure stays zero at the outlets and the diameter stays constant. This confirms that the outlet conditions behave as intended and that there no interaction with the solid.

The inlet pressure seems to be slowly converging back to 0 after the pulse has passed.

This results in a slight pressure difference between the outlets, set to zero pressure, and the inlet. It seems that this causes flow from the carotid arteries down the descending aorta (figure 13d), as the flow is not allowed to go through the inlet. This is most likely an artifact of the unphysiological boundary conditions.

Computational Solid Mechanics

A uniform pressure of 8000 Pa $\simeq$ 60 mmHg was set on the inner surface of the wall. A steady state calculation was carried out. For every increment of the solution the pressure is increased until it hits the intended pressure, being the solution to the steady state problem. A sudden increase in pressure, i.e. a step function, would be very hard to calculate.

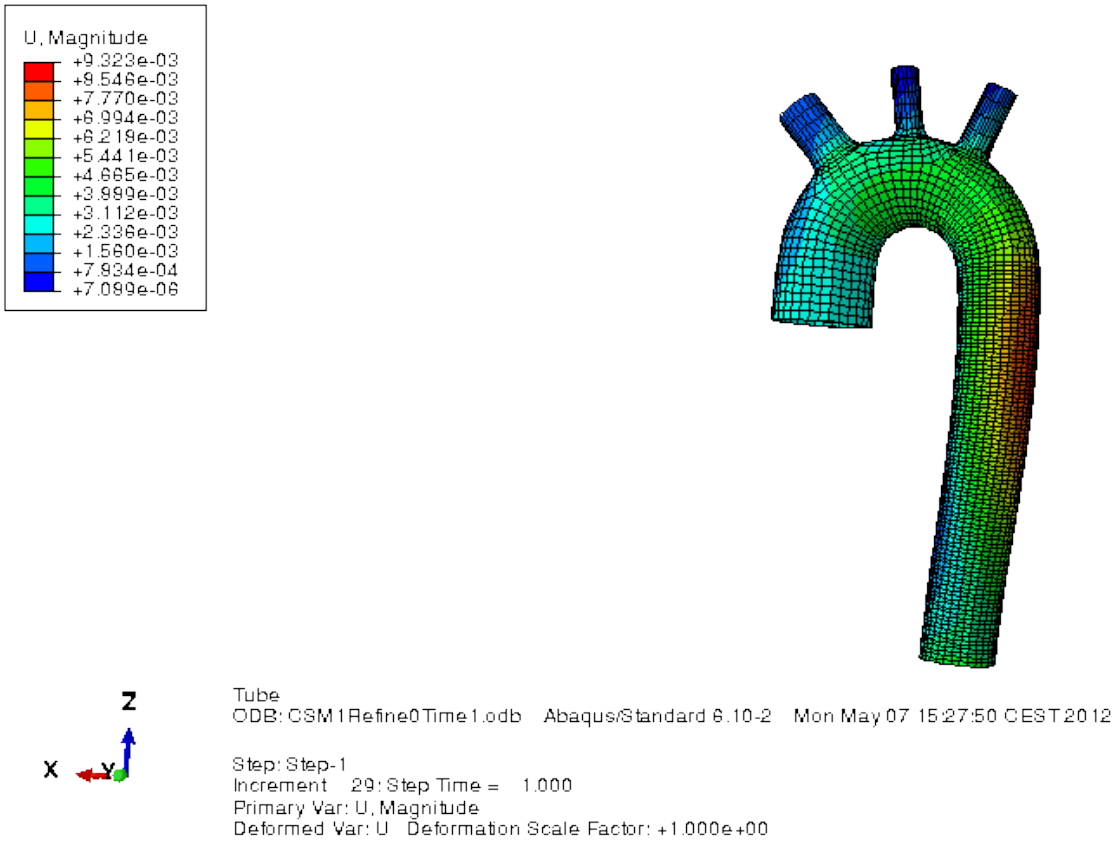

Figure 14: Plots for the deformation of the aortic arch from the side. Steady state calculation with a uniform pressure of 8000 Pa. $\Delta t = 0.005$s.

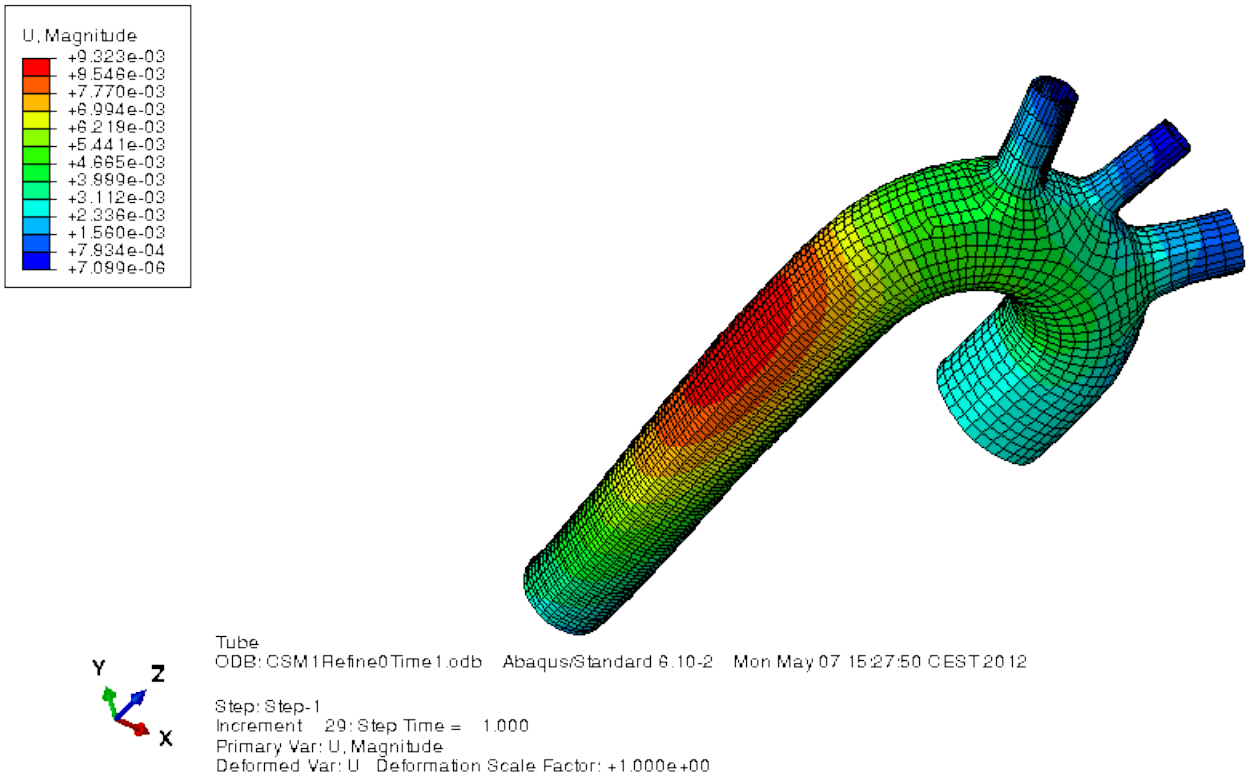

Figure 15: Plots for the deformation of the aortic arch from the back. Steady state calculation with a uniform pressure of 8000 Pa. $\Delta t = 0.005$s.

There is a uniform pressure inside the model and equal material parameters everywhere. There is a maximum displacement of 9.323 mm, which is on the descending aorta. This displacement is however not symmetrical, even though the pressure field is. The inlet and all of the outlets are set in the lengthwise direction, meaning that the aorta is basically expanding between two plates. The geometry inflates and since it is restriced by the outlets it will buckle outwards on the descending aorta. This leads to the wall extending furthest in the point of failure.

Fluid Structure Interaction

The FSI simulation did not run, claiming "Convergence error in Abaqus" before any subiterations have completed. Abaqus returns error code 16, which is "An Unexpected Error". This is a general error message without a distinct cause. The problem seems to be mesh dependent as the same meshes repeatedly gets this error, while other meshes, of different geometries, never receive it. This is despite several modifications to parameters and boundary conditions. Since no iterations complete the physics of the problem should not be able to pose a problem. Hypothesized causes are mesh quality or the numbering methods Ansys Workbench employ, which may conflict with the coupling code. These are however just guesses. Mesh quality was improved, but what should be adequate meshes (Max skewness 0.7) still gets the same error. Attempts at creating two similar cases where

one works and the other does not, for troubleshooting purposes, have been unsuccessful. The differences of these cases could then be examined more thoroughly. In order to create one case that doesn't work and another that does with differences that are easily studied, it is beneficial to know what the problem is beforehand.

The problem could be persisting in the cases that do run, but isn't prominent enough to affect the solution significantly. This will hopefully be looked at in future work as it was not resolved during this project.

5.3 Simple Arch

Case 1 Results for the simplest arch case studied.

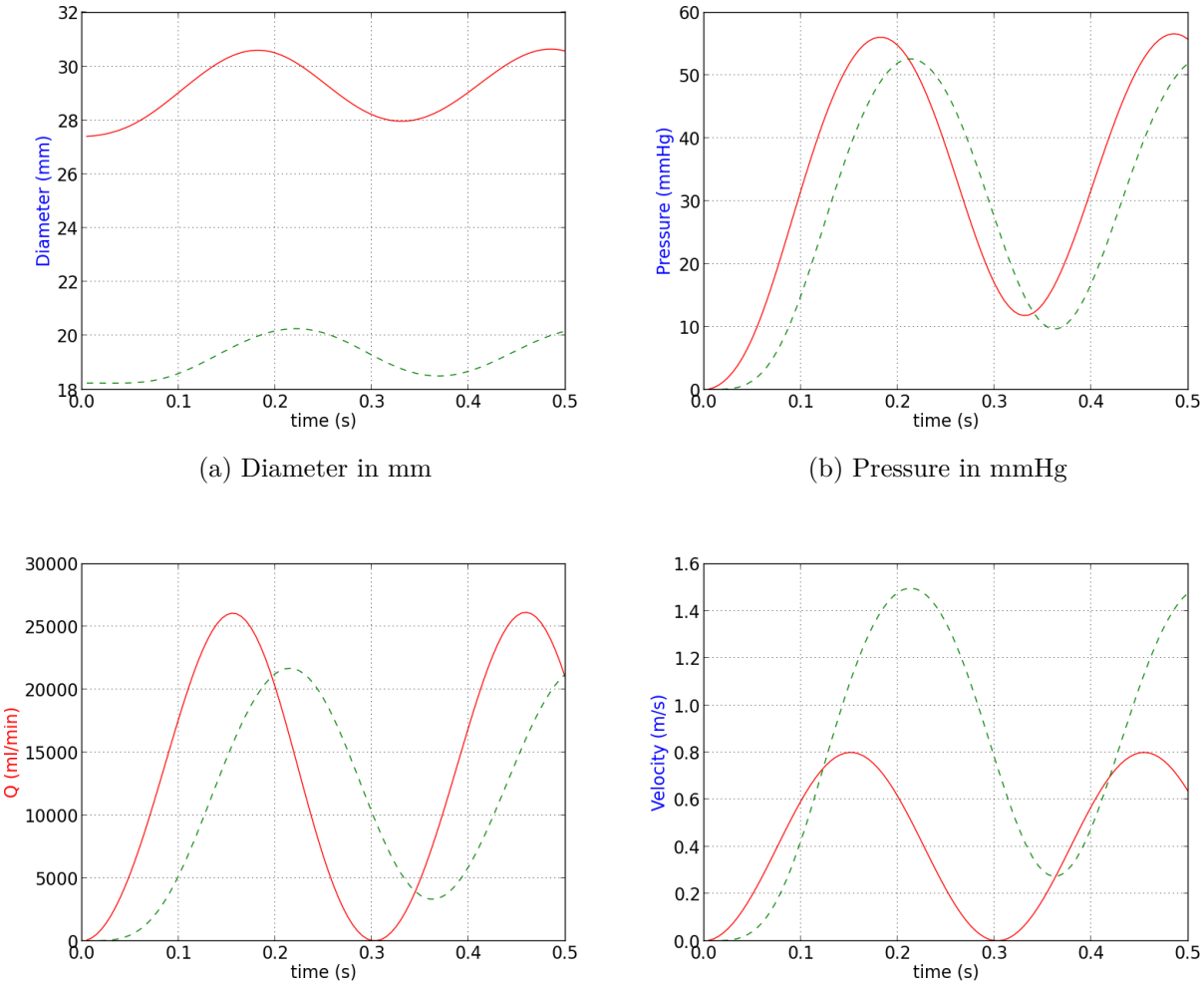

(a) Diameter in mm

(b) Pressure in mmHg

(c) Massflow in ml/min

(d) Velocity in m/s

Figure 16: 2D plots of 4 different parameters as a functions of time for each of the boundaries: Inlet [red], outlet [green - -]. $\Delta t = 0.005$s.

There is no reflection at the outlet, which was the intention of the boundary condition. There is a pressure build up at the outlet since the initial pressure is set to 0, and it takes

some time to adjust to the massflow periodically entering the vessel.

Case 2 The simulation would not converge. A velocity inlet condition is a strict condition and the complexity of the profile could be a problem for the solution.

Case 3 The 3WK model uses the pulse wave velocity c in calculating the characteristic impedance used as a resistance factor. The PWV is a material property and a function of pressure. The definition is given in eq 26.

$$c = \sqrt{\frac{A}{\rho}\frac{dP}{dA}} \tag{26}$$

To find the wavespeed a calculation of the solid mesh was performed with a uniform pressure distribution. This was done in much the same way as the CSM calculation in section 5.2, but for a larger pressure. From this the wavespeed for a range of pressures was found. The results are given in figure 17. A second order polynomial was used to approximate the solution on the outlet and transfered to the FSI simulation.

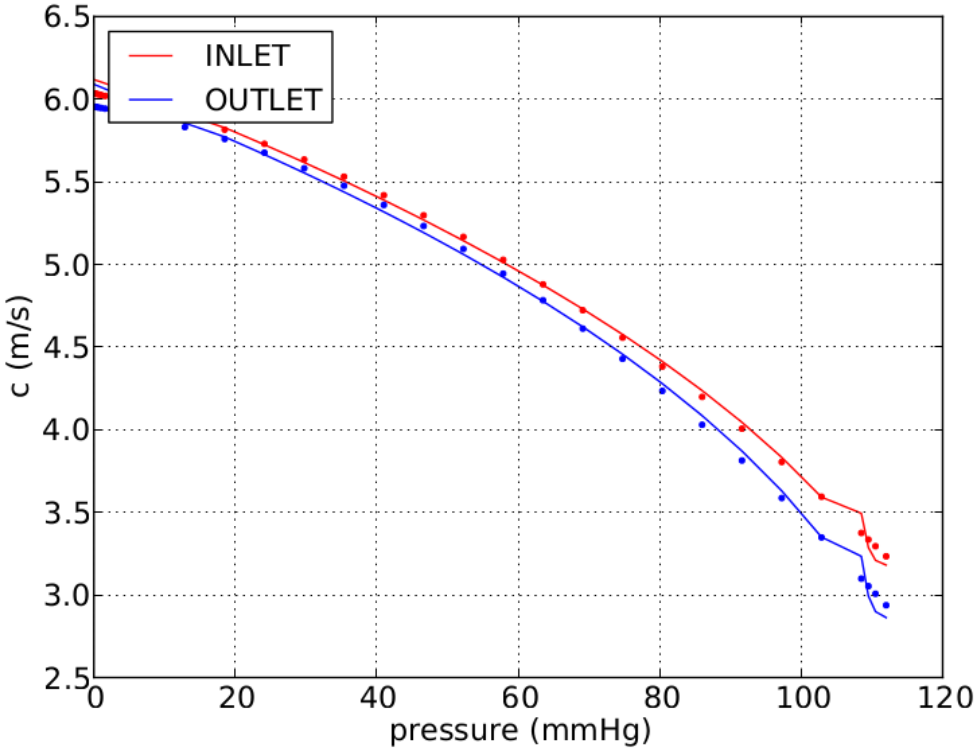

Figure 17: Wavespeed approximation from steady state FEM simulations for a range of pressures with calculated values [–] and polynomial approximation [.].

The drop in c is because of the linear wall elasticity. For a hyperelastic wall condition the wavespeed would grow exponentially as a higher pressure would meet more resistance.

The literature [4,8,11,13] gives different possible parameters for the Windkessel model, even for similar simulations. Basing our Windkessel on the method used in Beulen et al. [3], see sec. 2.2, with a mean pressure of 100 mmHg and mean flow of 94.3 ml/s we get the parameters stated in table 4. The mean flow is calculated for a $\sin^2$ wave with 450 ml/s as amplitude, frequency 2.77 s^{-1} and pause of 0.5 s between pulses.

Table 4: Parameters for the 3 element Windkessel model applied on the outlet

Parameter	**Value**
R [mmHg s/ml]	0.935
C [ml/mmHg]	1.604

The simulation is run for a long time to allow the pressure in the Windkessel model to build up. The buildup is shown in fig. 18. After a while the solution stabilizes into a periodic pattern. The results are shown in fig. 19. The simulation was run with convergence criteria of 1e-6 and timestep of 20 ms.

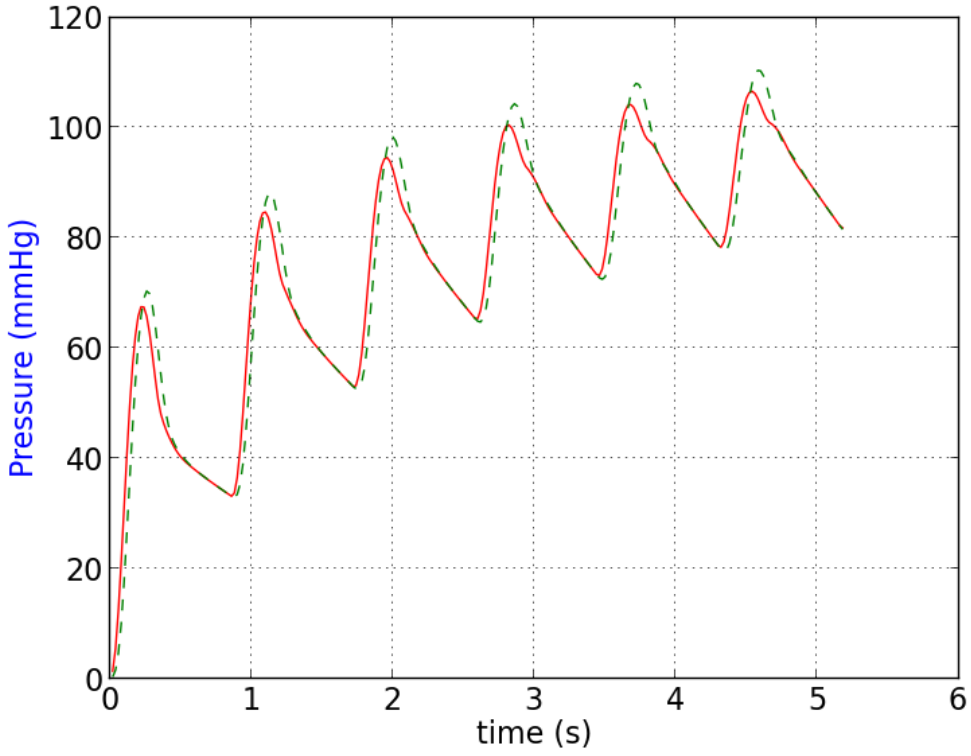

Figure 18: Pressure at the inlet [red] and outlet [green - -] for the pressure buildup period of the Windkessel model.

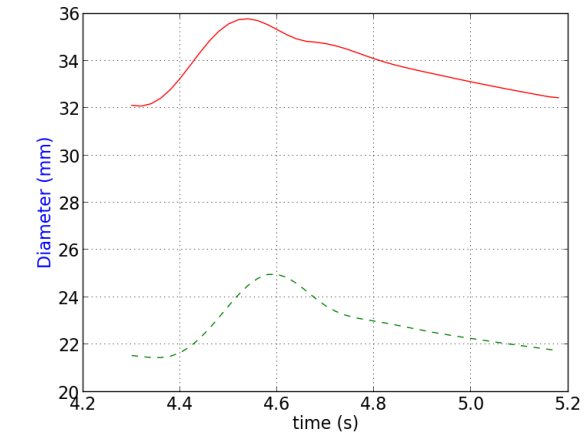

(a) Diameter in mm

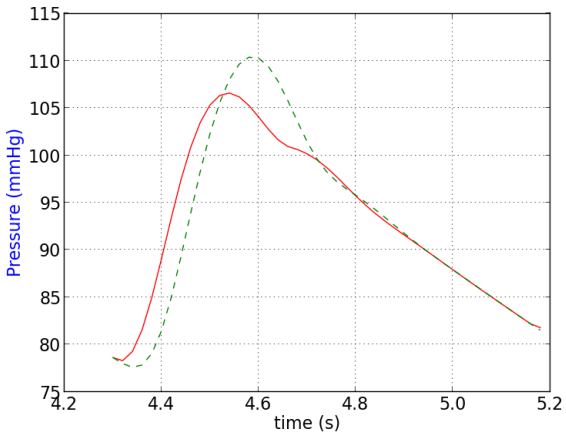

(b) Pressure in mmHg

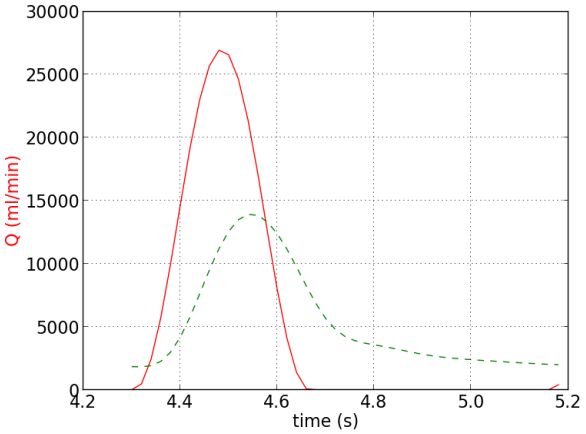

(c) Massflow in ml/min

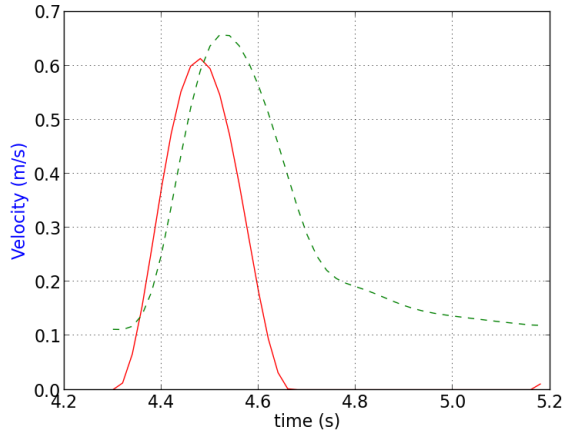

(d) Velocity in m/s

Figure 19: 2D plots of 4 different parameters as a function of time for each of the boundaries: Inlet [red], outlet [green - -]. Plots are of one iteration of the periodic solution. $\Delta t = 0.02$s

The pressure has built up to a physiological range of 80 - 110 mmHg. We can see a dip in the pressure when the influx of blood ceases. This resembles the dicrotic notch, which occurs in physiological flow when the heart valve closes. This would most likely be more prominent with a more accurate inflow condition.

Because of the mass flow inlet condition, the flow at the inlet is prescribed and will not adapt to the flow conditions inside the domain. Backflow is not possible if not set in the profile. This means that we have also decided, before the simulation, what reflections we allow at the inlet.

Figures 20 and 21 show vector plots and contour plots respectively of the simplified arch at 4 separate timesteps. This is shown to give an idea of how the pressure wave travels through the domain and how this affects the velocity.

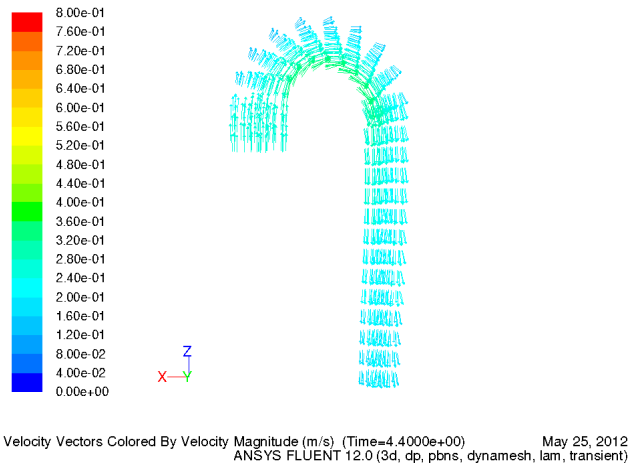

(a) Time: 4.4 s

(b) Time: 4.5 s

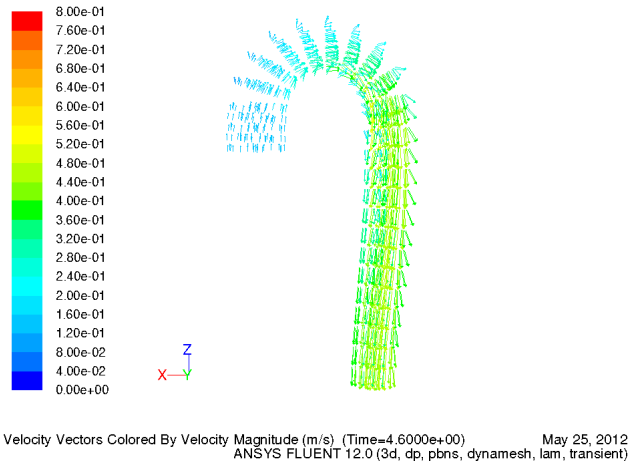

(c) Time: 4.6 s

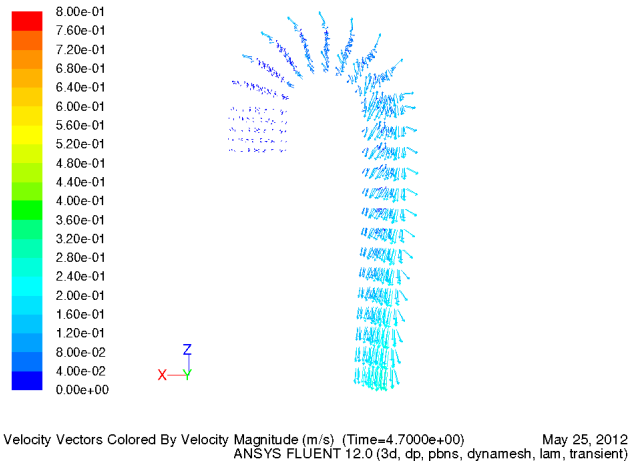

(d) Time: 4.7 s

Figure 20: Vector plots at different timestep. Colors denote velocity magnitude from 0 m/s to 0.8 m/s. $\Delta t = 0.02$s.

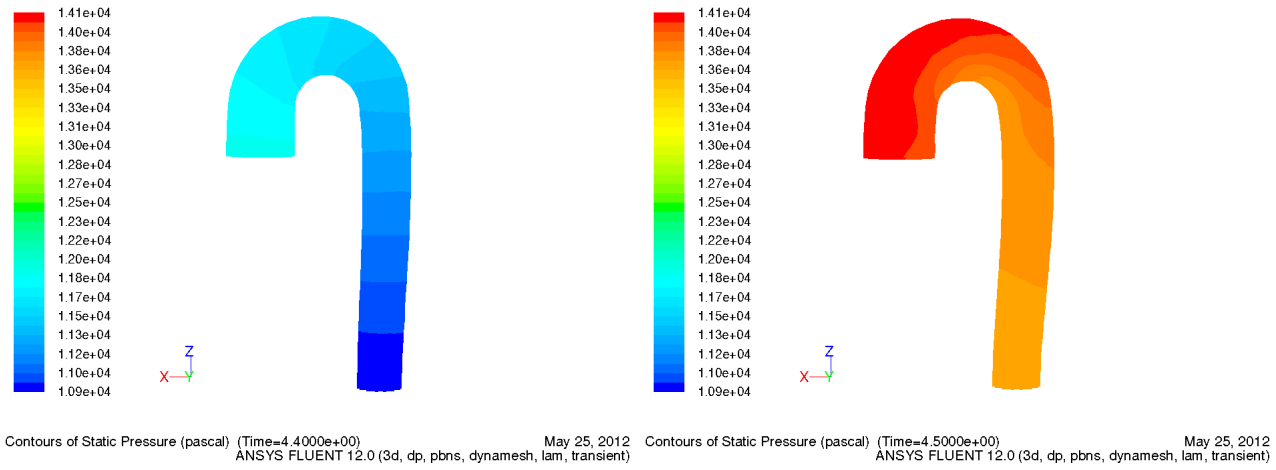

(a) Time: 4.4 s

(b) Time: 4.5 s

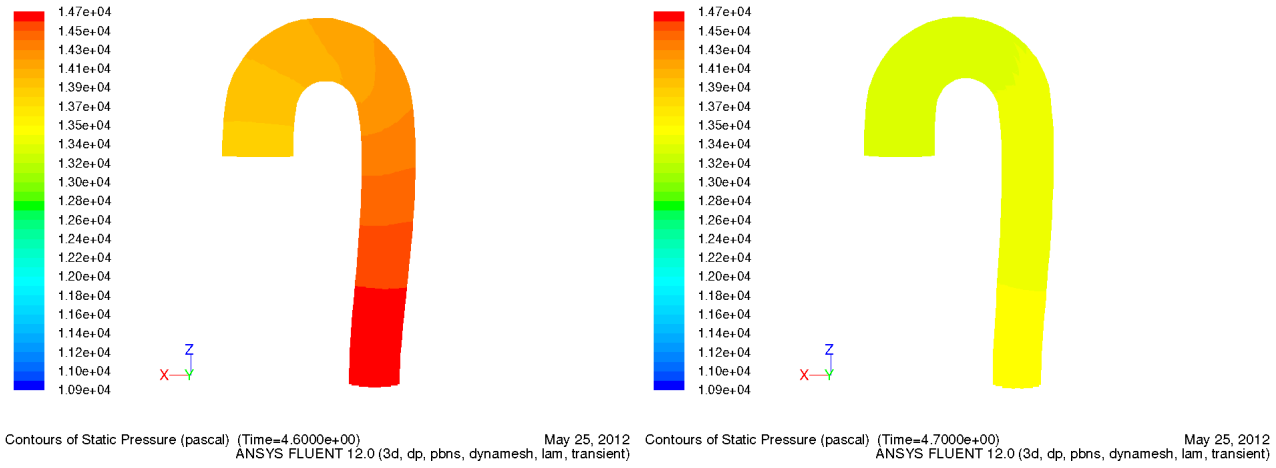

(c) Time: 4.6 s

(d) Time: 4.7 s

Figure 21: Contour plots at 4 different timesteps. Colors denote pressure from 80 mmHg to 110 mmHg in Pa. $\Delta t = 0.02$s.

Case 4 For the resistance model the results are given below. Figure 22 shows that there is only a slight buildup of pressure, while figure 23 shows the results from a single pulse at the end of the simulation.

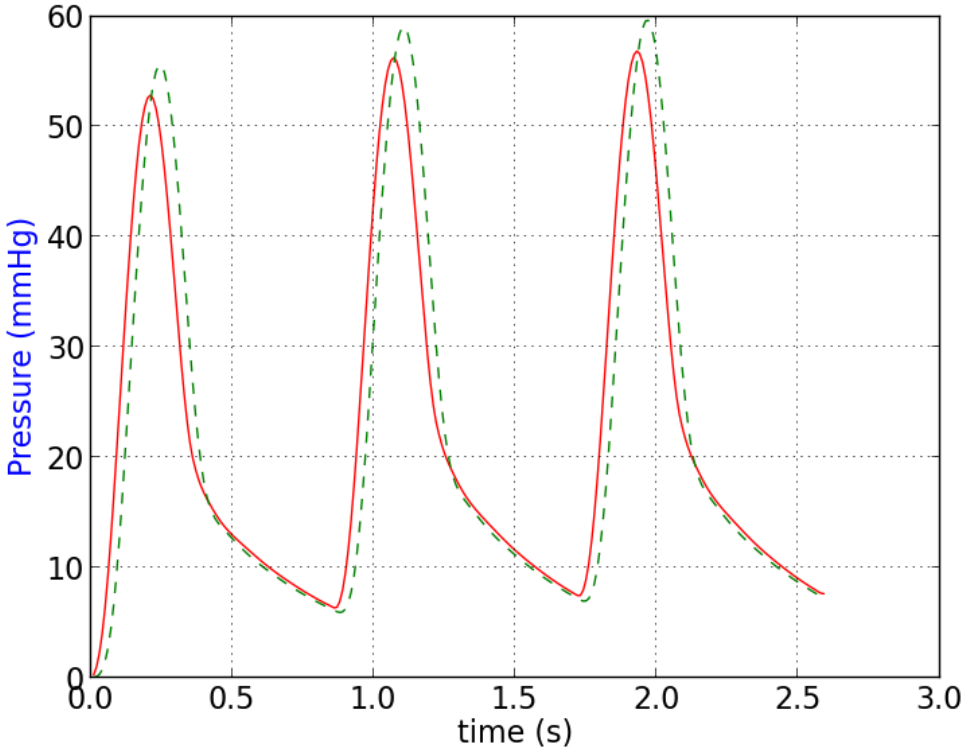

Figure 22: Pressure history of the simulation for the inlet [red] and outlet [green –]. There is hardly any buildup in the outlet model.

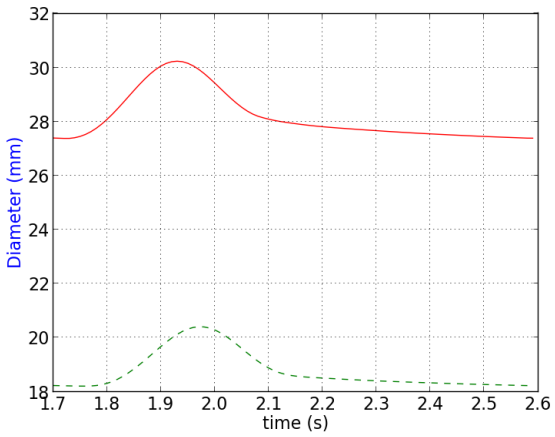

(a) Diameter in mm

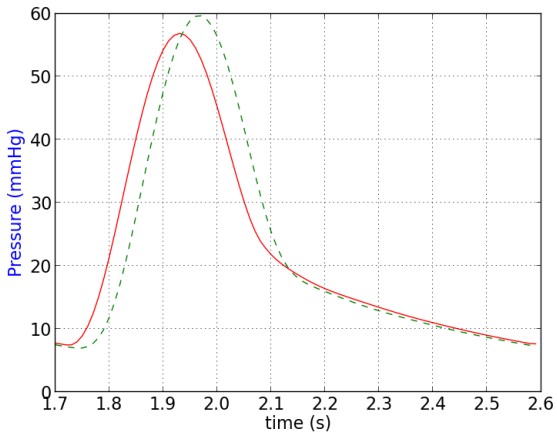

(b) Pressure in mmHg

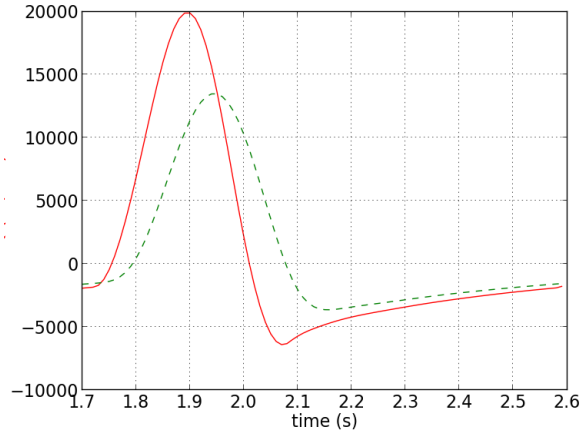

(c) Massflow in ml/min

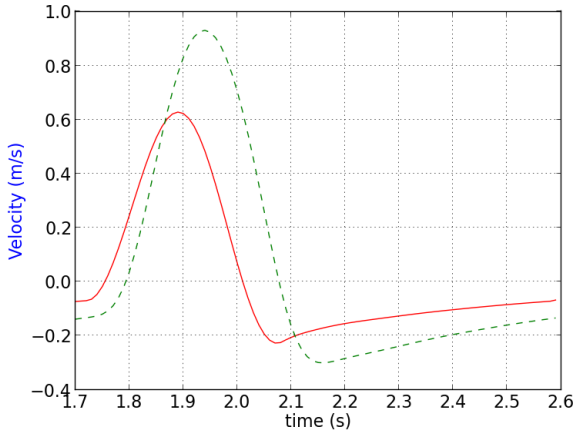

(d) Velocity in m/s

Figure 23: 2D plots of 4 different parameters as a function of time for each of the boundaries: Inlet [red], outlet [green - -] $\Delta t = 0.01$s.

With this resistance model there is only a slight buildup of pressure inside the vessel. After the pulse passes there is no pressure at the inlet. Because of the resistance of the Windkessel model the outlet pressure is not zero. We therefore have a gradient from the outlet to the inlet. When the flow reaches the inlet the resistance there will reflect some, but not all of it. This means that blood is allowed to flow back into the heart. The blood will basically slosh back and forth rather than be pushed through the system. If we increase the resistance to allow less blood back into the heart, the ventricular pressure needed to pass through the resistance at the inlet would need to be unphysiologically large. The source resistance, R_s, needs to be varying in time on order to use this method, as the average value used here does not model any physical feature of the flow and does not produce physiological results.

In the simulation we have run there is a slightly smaller peak mass flow than case 3, but is within physiological ranges. The pressure is not however as the inlet does not

force blood to accumulate in the vessel, thereby raising the pressure to push through the peripheral resistance in the Windkessel.

Case 5 The solution did not progress further than 0.41 seconds. At this point it seems that the subiterations hit backflow at the outlet and did not converge.

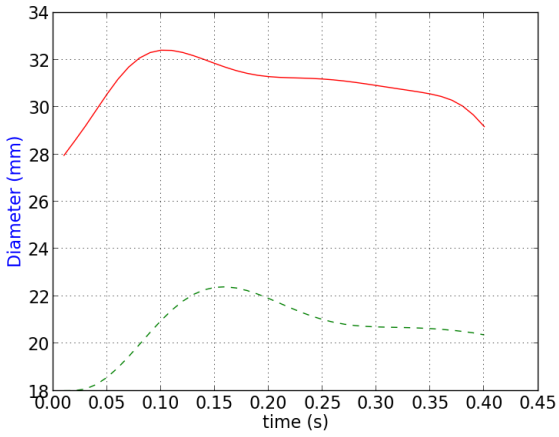

(a) Diameter in mm

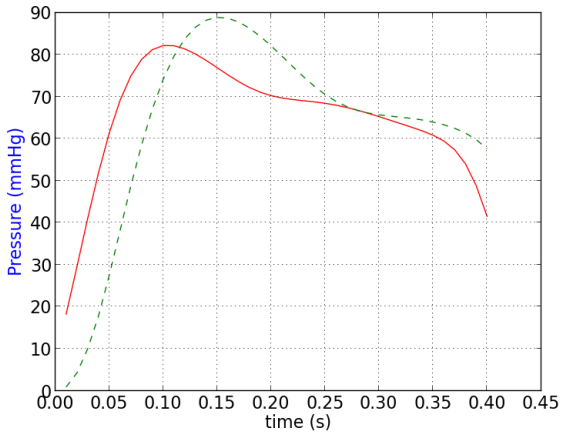

(b) Pressure in mmHg

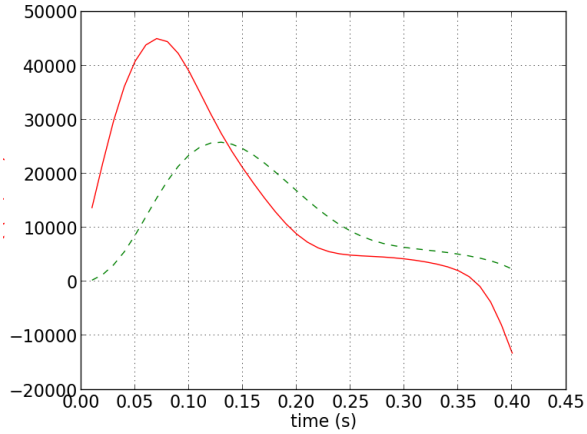

(c) Massflow in ml/min

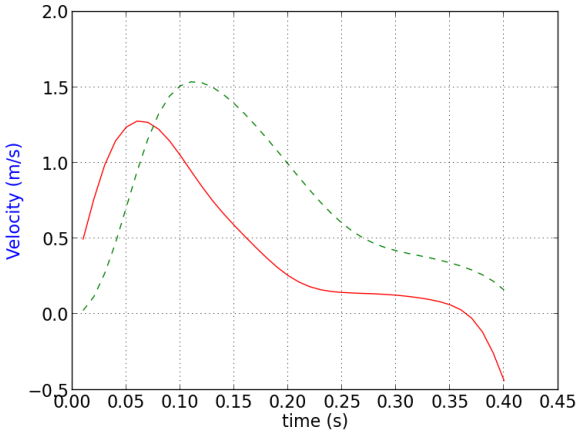

(d) Velocity in m/s

Figure 24: 2D plots of 4 different parameters as a function of time for each of the boundaries: Inlet [red], outlet [green - -] $\Delta t = 0.01$s.

It is difficult to get any information without seeing how the solution progresses. The initial pulse from the heart model has a much higher peak than the earlier simulations, and the pressure is lower than expected for physiological conditions. The inlet pressure as given here represents the ventricular pressure since no valve approximation was favorably implemented.

5.4 Convergence

Convergence was a problem throughout the project. This was mostly a problem when there was backflow on the outlet. When the flow was about to reverse flow vectors could line up with the outlet, as shown in figure 25. If this happened the solution would not converge.

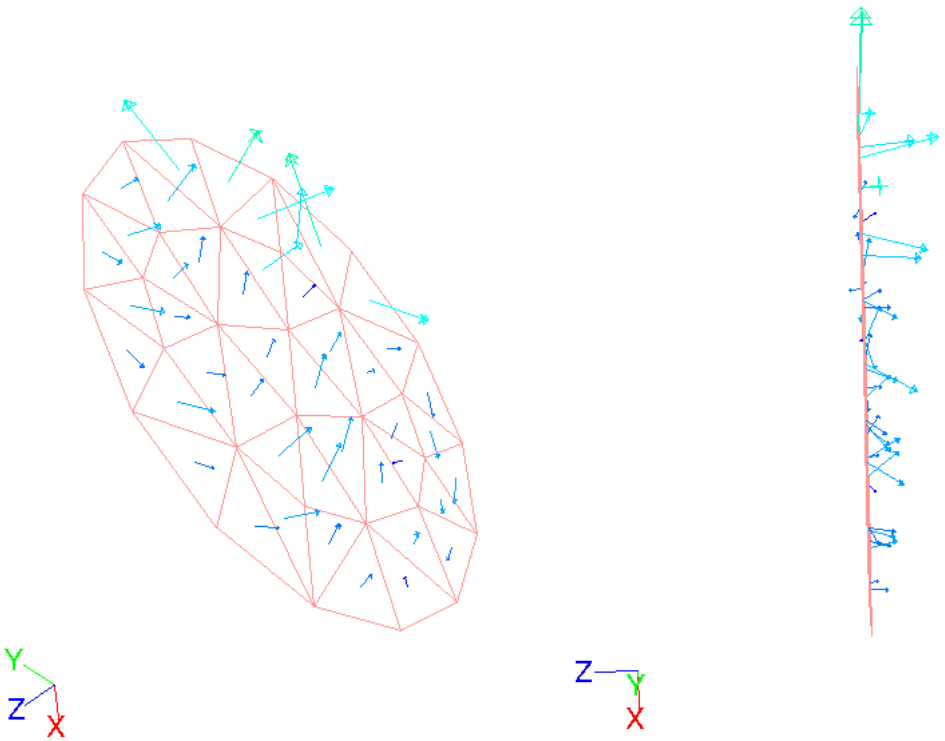

(a) Perspective view

(b) Side view

Figure 25: Vectors on the outlet for a non-converging solution. The vectors are lining up with the outlet plane.

This problem did not occur for all instances of backflow, as some simulations seemed to move past this without incident. This was mostly an issue with cases 3, 4, and 5 on the simplifed geometry since these cases included backflow on the outlet.

This problem does not affect the succesful simulations. Either the simulations ran smoothly or did not converge. There would be no adverse effects on the simulations that converged, as the problem would not present itself.

6 Conclusion

The simplified model was simulated for several cases with different boundary conditions. The mass flow condition produces nearly physiological responses as it is modeled as an approximation of the mass flow produced by the heart motion. All reflections at the inlet are predetermined as these must fit with the inlet condition. This requires an accurate, patient specific profile for every pathological case that needs to be studied.

The resistance model inlet produced too little resistance to backflow after the initial pressure pulse. The pressure did not build up to expected ranges as the blood would just flow back out of the inlet. This is because the resistance was constant through the cycle, and not changing in accordance with a valve motion. The resistance at the inlet does therefore not represent any physical mechanism, and was in that regard a poor model.

A time-varying elastance approach represents a potential of easily adapting the inlet to different healthy and pathological conditions, with changes to the parameters. However, because of convergence issues no conclusions can be drawn regarding this in our study. The lack of an accurate expression for flow in and out of the left ventricle and lack of valve produced results differing from the literature.

Results were not obtained for the full model, so it had to be simplified in order to continue the investigation. The full model's inability to run was not resolved. The cause of the problem has not been found, but is most likely connected to the mesh as other meshing tools have functioned in conjunction with Tango earlier. The problem also seemed to stay with the meshes, i.e. if a mesh recieved the error message it would not run for any other conditions or alterations.

No conclusion can be drawn on the viability of Ansys Workbench as a meshing tool for Tango simulations. There were startup issues with some meshes, but not all of them. Since the root cause of this could not be found ruling out Ansys Workbench would be premature.

Epilogue: A physiological aortic arch was constructed from MRI measurements, modeled and meshed by Kamil Rehak. The mesh was created with Ansys ICEM, and attempted simulated. However the simulation gave the same error message as the full idealized model, section 5.2.

7 Further Work

As the FSI simulation of the full arch, including bifuractions, did not run the logical next step is to figure out why this is and get it working. This could include meshing with another software, which has worked in other studies. It would, on the other hand, be beneficial to find out why this mesh generation was unsuccesful, if that is the problem. In addition a model of a patient specific aortic arch has been constructed and should

be simulated. This a much more complicated geometry, but gives greater insight into to the physics in a true human aorta as opposed to our simplified model. If a quantitative analysis is to be run mesh independence needs to be examined and the mesh refined in areas of larger gradients. The addition of turbulence models shoudl also be considered.

The varying elastance model should be examined to see if it is a viable option. This would probably include separating forward and backward travelling waves at the inlet and finding a way of refilling the cavity volume.

The goal of this study was to lay the groundwork for future studies on aortic dissection. Pathological flow should be examined, looking at hypertension, stenosis and/or weaknesses in the aortic wall to see how these affect the forces leading to the development of aneurysms or dissection. Gao et al. [6] uses the wall shear stress as an indicator of dissection risk.

There is also work on a 1 dimensional arterial network code. Crosetto et al. [4] uses 1D solutions as outlet conditions on the FSI simulation and this could possibly be implemented in the current framework.

References

[1] *Fluent User's Guide 14*.

[2] *Tango Manual*.

[3] B. Beulen, M. Rutten, and F. van de Vosse. A time-periodic approach for fluid-structure interaction in distensible vessels. *Journal of Fluids and Structures*, 25:954–966, 2009.

[4] P. Crosetto, P. Reymond, S. Deparis, D. Kontaxakis, N. Stergiopulos, and A. Quarteroni. Fluid-structure interaction simulation of aortic blood flow. *Computers and Fluids*, 43:46–57, 2011.

[5] J. Degroote. *Development of Algorithms for the Partitioned Simulation of Strongly Coupled Fluid-Structure Interaction Problems*. PhD thesis, Ghent University, 2010.

[6] F. Gao, M. Watanabe, and T. Matsuzawa. Stress analysis in a layered aortic arch model under pulsatile blood flow. *BioMedical Engineering OnLine*, 5:1–11, 2006.

[7] D. Juang, A. C. Braverman, and K. Eagle. Aortic dissection. *Circulation*, 118:507–510, 2008.

[8] J. Lantz, J. Renner, and M. Karlsson. Wall shear stress in a subject specific human aorta. *International Journal of Applied Mechanics*, 4:759–778, 2011.

[9] P. R. Leinan, J. Degroote, T. Kiserud, B. Skallerud, and L. R. Hellevik. Velocity profiles in the human ductus venosus: a numerical fluidstructure interaction study. Ongoing research, 2012.

[10] G. R. Liu and S. S. Quek. *The Finite Element Method: A Practical Course*. Butterworth - Heinemann, 2003.

[11] P. Moireau, N. Xiao, M. Astorino, C. A. Figueroa, D. Chapelle, C. A. Taylor, and J.-F. Gerbeau. External tissue support and fluid-structure simulation in blood flows. *Biomech Model Mechanobiol*, 11:1–18, 2012.

[12] P. Mynard, M. R. Davidson, D. J. Penny, and J. J. Smolich. A simple, versatile valve model for use in lumped parameter and one-dimensional cardiovascular models. *Int. J. Numer. Meth. Biomed. Engng.*, 10:1–16, 2011.

[13] N. M. Pahlevan and M. Gharib. Aortic wave dynamics and its influence on left ventricular workload. *PLoS ONE*, 6:1–2, 2011.

[14] A. Redheuil, W. Yu, E. Mousseaux, A. Harouni, N. Kachenoura, C. Wu, D. Bluemke, and J. Lima. Age-related changes in aortic arch geometry. *Journal of the American College of Cardiology*, 58:12, 2011.

[15] N. Stergiopolus, D. F. Young, and T. R. Rogge. Computer simulation of arterial flow with applications to arterial and aortic stenoses. *Journal of Biomechanics*, 25:1477–1488, 1992.

[16] H. Suga and K. Sagawa. Mathematical interrelationship between instantaneous ventricular pressure-volume ratio and myocardial force-velocity relation. *Annals of Biomedical Engineering*, 1:160–181, 1972.

[17] T. T. Tsai, A. Evangelista, C. A. Nienaber, T. Myrmel, G. Meinhardt, J. V. Cooper, D. E. Smith, T. Suzuki, R. Fattori, A. Llovet, J. Froehlich, S. Hutchison, A. Distante, T. Sundt, J. Beckman, Jr. J. L. Januzzi, E. M. Isselbacher, and K. A. Eagle. Partial thrombosis of the false lumen in patients with acute type b aortic dissection. *New England Journal of Medicine*, 357:349–359, 2007.

Lists

List of Figures

List of Tables